



DEPARTMENT OF MARINE TECHNOLOGY

TMR4240 - MARINE CONTROL SYSTEMS I

Final Project : Design of Dynamic Positioning System

Authors:

Abdelhaleem Osman Abdelhaleem Saad
Ahmed Abdallah Abdelrehim Abdelgayed
Ramy Antar Ahmed Alham
Zhongyu Zhang

November 12, 2023

Table of Contents

List of Figures	ii
List of Tables	v
1 Introduction	1
2 Process plant model	1
3 Control plant model	3
3.1 Low-frequency control plant model	3
3.2 Wave-frequency control plant model	4
3.3 Bais model	4
3.4 Measurement model	5
3.5 Complete control plant model	5
4 Wind Model	5
4.1 Implementation	5
5 Wave Model	6
6 Current model	6
7 Reference Model	7
7.1 Mathematical Model	7
7.2 Tuning Values	8
7.3 Simulink Diagram	8
8 Observer design	9
8.1 Extended Kalman Filter Design	10
8.1.1 Implementation	11
8.1.2 Tuning values	11
8.2 Non-linear Passive Observer	12
8.2.1 Observer Model Description	12
8.2.2 Observer Equations	12
8.3 Determination of the Observer Gains	12
8.3.1 Observer Gain Tuning	13
9 Thrust Allocation	13

9.1	Thrust Allocation Overview	13
9.1.1	Mathematical Model	13
9.2	Methods used	14
9.3	Optimization Process for Pseudoinverse vs. Quadratic Programming	15
9.3.1	Constraints	16
10	Controller design	19
10.1	Tuning of the PID controller	20
11	Simulation Results	21
11.1	Part 1	21
11.1.1	Simulation 1	22
11.1.2	Simulation 2	24
11.1.3	Simulation 3	26
11.1.4	Simulation 4	27
11.2	Part 2	32
11.2.1	Simulation 1 - Environmental Loads	32
11.2.2	Simulation 2 - DP and Thrust Allocation	34
11.2.3	Simulation 3 - DP and Environmental Forces	44
11.2.4	Simulation 4 - Observer selection	46
11.2.5	Simulation 5 - Complete Simulation	49
11.2.6	Simulation 6 - Capability Plot	51
11.2.7	Simulation 7 - Observer robustness	53
12	Conclusion	57
References		58

List of Figures

1	Overview of the system	1
2	implementation of wind model with variation in magnitude and direction.	6
3	Wave Model	6
4	Implementation of current model with variation in magnitude and direction.	7
5	Simulink representation of the reference model.	9
6	Simulink representation of the reference model with switching mechanism.	9
7	Schematic of the Extended Kalman Filter implementation.	11

8	Non-linear Passive Observer, with the bias estimator model on the left, the wave estimator model on the right, K_2 representing kinematics, and the other components representing the dynamics of low-frequency motion.	12
9	Illustration of the three types of thrusters.	14
10	Thrust allocation methods used.	15
11	Dividing the azimuth force into x and y components.	16
12	Our Matlab Algortihm for Thrust allocation using the Pseudoinverse method.	17
13	This figure represents the position of the vehicle in the NED frame when disturbed by fixed current of magnitude $0.5m/s$ in the South-East direction. The red curve denotes the motion in East-axis, while the blue curve denotes the vehicle's motion in the North-axis.	22
14	This figure represents the Orientation of the vehicle in the NED frame when disturbed by fixed current of magnitude $0.5m/s$ in the South-East direction	23
15	This figure represents a XY-plot the shows both position and heading of the vessel in the NED frame when disturbed by fixed current of magnitude $0.5m/s$ in the South-East direction. The North-East position is indicated by the blue curve, while the heading is represented by the red arrows. Heading samples is taken every 1000 measurements.	23
16	This figure represents the position of the vehicle in the NED frame when disturbed by fixed current of magnitude $0.5m/s$ and varying direction from south to west direction. The red curve denotes the motion in East-axis, while the blue curve denotes the vehicle's motion in the North-axis.	24
17	This figure represents the Orientation of the Vessel in the NED frame when disturbed by Varying current of fixed magnitude $0.5m/s$ and varying direction from south to west	25
18	This figure represents a XY-plot the shows both position and heading of the vessel in the NED frame when disturbed by fixed current magnitude $0.5m/s$ and varying current direction. The North-East position is indicated by the blue curve, while the heading is represented by the red arrows. Heading samples is taken every 1000 measurements.	25
19	This figure represents the DP performance in making the vehicle move from $\eta_0 = [0, 0]$ to $\eta_{SP} = [10, 10]$ with and without reference model.	26
20	This figure represents the DP performance in making the vehicle change its heading from $\psi_0 = [0]$ to $\psi_{SP} = [3\pi/2]$ with and without reference model.	26
21	This figure represents the DP performance represented by xy-plot in making the vehicle change its state from $\psi_0 = [0, 0, 0]$ to $\psi_{SP} = [10, 10, 3\pi/2]$ with and without reference model. The Red arrows represent the vessels heading while the blue line represents the path in the xy-plane.	27
22	This figure represents the position of the vehicle in the NED frame following a set of desired points without any environmental disturbances. The red curve denotes the motion in East-axis, while the blue curve denotes the vehicle's motion in the North-axis. The text boxes provide information about maximum overshoot happening in the system's position, while the arrows are pointing at regions of interest to be discussed and explained.	28
23	This figure represents the heading of the vehicle in the NED frame following a set of desired points without any environmental disturbances. The text boxes provide information about maximum overshoot happening in the system's heading, while the arrows are pointing at regions of interest to be discussed and explained.	29

24	The following figure represents the xy-plot of the vehicle following the desired state. It shows arrows that represent the transition between states in NED frame. The boxes show maximum overshoot happening.	30
25	The following figure represents the xy-plot of the vehicle following the desired state. It shows arrows that represent the heading of the vessel, ψ	31
26	Plots demonstrating the vessel's response to environmental loads inheading, position, and overall trajectory.	32
27	Drifting the vehicle under strong wind in south East	33
28	Performance of thrust allocation in various axes for quadratic programming	34
29	the output thrust u for all the thrusters for quadratic programming	35
30	Observed thrust directions (Alpha) in various thrusters over time for quadratic programming.	36
31	XY plot showing the ship's actual trajectory against the desired trajectory using quadratic programming.	37
32	pseudo-inverse Performance of the thrust allocation in various Axeses	38
33	the output thrust u for all the thrusters for pseudo-inverse	39
34	Observed thrust directions (Alpha) in various thrusters over time for Pseudo inverse.	40
35	XY plot showing the ship's actual trajectory against the desired trajectory using pseudo inverse.	41
36	Performance of the thrust allocation in various Axeses when the thruster number 2 and 4 are disabled.	42
37	The output thrust u for thrusters 1, 3, and 5 when thrusters 2 and 4 are disabled.	43
38	XY plot showing the ship's actual trajectory against the desired trajectory when the thruster numbers 2 and 4 are disabled.	44
39	Rotational motion plot showing the actual trajectory in comparison to the desired trajectory.	44
40	Translational motion plot for x and y.	45
41	XY plot of the vessel's trajectory. The actual trajectory is marked in blue, and the desired trajectory in red, with arrows indicating the direction of movement.	45
42	Comparison of the North, East, and Psi components of the observer output with the real measurements under full environmental forces. The Extended Kalman Filter (EKF) and Nonlinear Passive Observer (NPO) are plotted against the true values (Real) showing the tracking performance over time.	46
43	Velocity estimation graphs for North, East, and Psi components, including the influence of wave forces. Both the EKF and NPO observers are compared against the real measurements, illustrating the effect of environmental disturbances on velocity estimation.	47
44	XY-plot of observer outputs for path tracking with wave forces included. The plot demonstrates the path tracking accuracy of the EKF and NPO observers compared to the real trajectory.	47
45	Comparison of the North, East, and Psi components of the observer output with the real measurements without considering waves forces/moment. The Extended Kalman Filter (EKF) and Nonlinear Passive Observer (NPO) are plotted against the true values (Real) showing the tracking performance over time.	48

46	Velocity estimation graphs for North, East, and Psi components, without the influence of wave forces. Both the EKF and NPO observers are compared against the real measurements.	48
47	XY-plot of observer outputs for path tracking without wave forces/moment. The plot demonstrates the path tracking accuracy of the EKF and NPO observers compared to the real trajectory.	49
48	Full DP system performance in the 4 corner test under full environmental loads, current, wind, and waves, using EKF as an observer. The figures shows vessel's state η (North, East , Psi) w.r.t desired state	50
49	XY plot showing the vessel's performance in the 4 corner test. The vessel's position is represented by blue curves while the heading is represented by red arrows. The desired path is plotted as orange-colored square. Arrows and circle's are pointing to areas of interest which are to be discussed.	51
50	Average Thrust Utilization Without Constraint	52
51	Average Thrust Utilization With Constraint	53
52	Full DP system performance in station keeping at $\eta = [000]$ test under full environmental loads, current, wind, and harsher waves, without observer. The figures shows vessel's position η (North, East) as blue curve and heading, represented by red arrows	54
53	Full DP system performance in station keeping at $\eta = [000]$ test under full environmental loads, current, wind, and harsher waves, using NPO as an observer. The figures show the vessel's position η (North, East) as a blue curve and heading, represented by red arrows	55
54	Full DP system performance in station keeping at $\eta = [000]$ test under full environmental loads, current, wind, and harsher waves, using EKF as an observer. The figures shows vessel's position η (North, East) as blue curve and heading , represented by red arrows	56

List of Tables

1	PID Controller Gains for Surge, Sway, and Yaw used in part 1	21
2	PID Controller Gains for Surge, Sway, and Yaw used in part 2	21

1 Introduction

This project, part of the TMR4240 Marine Control Systems 1 course, focuses on the design and implementation of a Dynamic Positioning (DP) system for a supply vessel. It encompasses various components

1. Reference model
2. Observer and wave filters
3. PID controllers
4. Thrust allocation
5. environmental models for wind, current and waves

In each section, we present the mathematical model and elaborate on its utilization within the system. To ensure the accuracy and functionality of the systems, extensive simulations will be conducted. The effectiveness and efficiency of the solution will be assessed based on simulation results. These simulations resemble the typical DP operations.

The development of this solution is carried out using Matlab and Simulink, utilizing the Marine Systems Simulator (MSS) library and a marine systems simulator.

Figure 1 provides an overview of the system, with the gray blocks indicating the specific components implemented as part of this project.

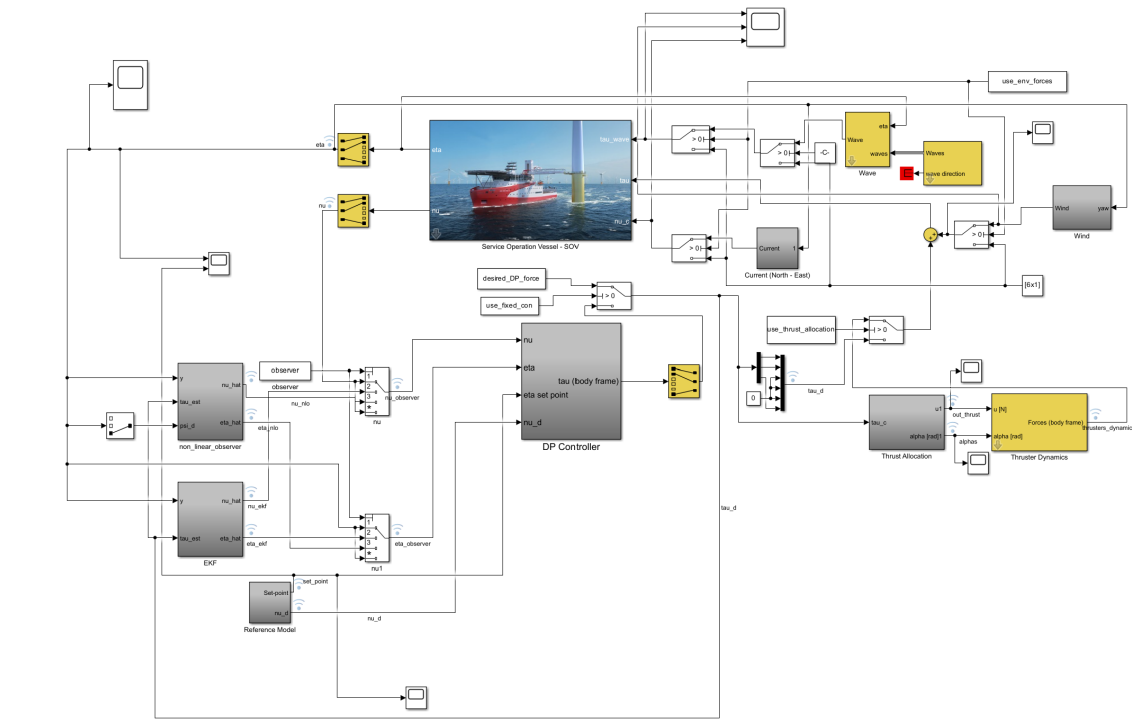


Figure 1: Overview of the system

2 Process plant model

A process plant model (PPM), or simulation model, is a comprehensive description of the actual process, incorporating as much detail as required using high-fidelity models. Its primary purpose

is to simulate the real plant dynamics, including environmental disturbances, control inputs and sensor outputs. A successful numerical simulation for design and verification of our control system require a sufficiently detailed mathematical model of the actual process. This section will focus on the formulation of process plant models. This involves modelling the following:

- Vessel dynamics
- External forces and moments
- Environmental loads (Waves, Wind, Current and Ice)
- Thruster/propeller forces
- Mooring forces (if applicable) acting on the vessel

Process plant models are usually obtained from either:

- First principles of physics (e.g. Newtons law)
- Empirical by experiments (system identification, observations, machine learning)

In this simulation, the detailed process plant model is provided with all the parameters and coefficients. The process plant model is a nonlinear 6 DOF Low-Frequency Model - Surge, Sway, Heave, Roll, Pitch, and Yaw. The dynamic equation of motion for the 6 DOF low-frequency model is given as:

$$\mathbf{M}\ddot{\boldsymbol{\eta}} + \mathbf{C}_{RB}(\boldsymbol{\nu})\boldsymbol{\nu} + \mathbf{C}_A(\boldsymbol{\nu}_r)\boldsymbol{\nu}_r + \mathbf{D}_{NL}(\boldsymbol{\nu}_r, \boldsymbol{\gamma}_r)\boldsymbol{\nu}_r + \mathbf{D}\boldsymbol{\nu}_r + \mathbf{G}\boldsymbol{\eta} = \mathbf{T}_{env} + \mathbf{T}_{moor} + \mathbf{T}_{thr} + \mathbf{T}_{ice} \quad (1)$$

$$\dot{\boldsymbol{\eta}} = \mathbf{J}\boldsymbol{\nu} \quad (2)$$

Where:

- $\boldsymbol{\eta}$ represents the position and orientation vector expressed in NED frame $\boldsymbol{\eta} = [x, y, z, \phi, \theta, \psi]^T$
- $\boldsymbol{\nu}$ represents the linear and angular velocities expressed in body frame, $\mathbf{v} = [u, v, w, p, q, r]^T$
- $\boldsymbol{\nu}_r$ is the relative velocity vector, $\boldsymbol{\nu}_r = [u - u_c, v - v_c, w, p, q, r]^T$. u_c and v_c are the horizontal components of the current.
- \mathbf{M} is the mass matrix and it contains the rigid-body mass and added mass.
- \mathbf{C}_{RB} is the rigid-body Coriolis matrix
- \mathbf{C}_A is the added coriolis matrix
- \mathbf{D}_{NL} is the 6-dimensional nonlinear damping vector
- \mathbf{D} is strictly positive linear damping matrix caused by linear wave drift damping and laminar skin friction
- \mathbf{G} is the hydrostatic vector and it contains the weight and buoyancy.
- $\mathbf{T}_{env} = \mathbf{T}_{wind} + \mathbf{T}_{wave2}$ is the environmental load
- \mathbf{T}_{moor} is the mooring forces (if applicable)
- \mathbf{T}_{thr} is the thruster forces
- \mathbf{T}_{ice} is ice load (if applicable)

3 Control plant model

A control plant model is a simplified mathematical description that includes only the main physical properties of the process model. The simplified model is used for controller design and observer design. , it is common to separate the modeling of marine vessels into a low-frequency (LF) model and wave-frequency (WF) model. For controller design, we only interested in LF model. However we consider both WF and LF models for observer design.

3.1 Low-frequency control plant model

This control plant model is a nonlinear LF 3 DoF model as we only consider the motion in surge, say and yaw. The centripetal and coriolis force are excluded along with the external forces. the equation of motion is written as follows:

$$\dot{\boldsymbol{\eta}} = \mathbf{R}(\psi)\boldsymbol{\nu} \quad (3)$$

$$\mathbf{M}\dot{\boldsymbol{\nu}} + \mathbf{D}\boldsymbol{\nu} + \mathbf{R}^T(\psi)\mathbf{G}\boldsymbol{\eta} = \boldsymbol{\tau} \quad (4)$$

Where:

- $\boldsymbol{\nu} = [u, v, r]^T$
- $\boldsymbol{\eta} = [x, y, \psi]^T$
- $\boldsymbol{\tau} = [\tau_x, \tau_y, \tau_\psi]^T$ is the control input vector

The control plant model is nonlinear due to the rotation matrix $\mathbf{R}(\psi)$, which is defined as:

$$\mathbf{R}(\psi) = \begin{bmatrix} \cos(\psi) & -\sin(\psi) & 0 \\ \sin(\psi) & \cos(\psi) & 0 \\ 0 & 0 & 1 \end{bmatrix}$$

For low-speed applications, the matrices are defined as follows:

Mass Matrix \mathbf{M} :

$$\mathbf{M} = \begin{bmatrix} m - X_{\dot{u}} & 0 & 0 \\ 0 & m - Y_{\dot{v}} & mxG - Y_{\dot{r}} \\ 0 & mxG - N_{\dot{v}} & Iz - N_{\dot{r}} \end{bmatrix}$$

Damping Matrix \mathbf{D} :

$$\mathbf{D} = \begin{bmatrix} -Xu & 0 & 0 \\ 0 & -Yv & -Yr \\ 0 & -Nv & -Nr \end{bmatrix}$$

Hydrostatic Matrix \mathbf{G} :

$$\mathbf{G} = \begin{bmatrix} -Xx & 0 & 0 \\ 0 & -Yy & 0 \\ 0 & 0 & -N\psi \end{bmatrix}$$

Hydrostatic forces (weight and buoyancy) can be neglected as we don't consider the vertical motion so that the weight and buoyancy force will cancel each other so the final control plant model is:

$$\mathbf{M}\dot{\boldsymbol{\nu}} + \mathbf{D}\boldsymbol{\nu} = \boldsymbol{\tau} \quad (5)$$

3.2 Wave-frequency control plant model

The WF model is written according to the following equation:

$$\dot{\xi}_w = A_w \xi_w + E_w w_w, \quad \eta_w = C_w \xi_w. \quad (6)$$

$\eta_w \in \mathbb{R}^3$ is the position and orientation measurement vector, $w_w \in \mathbb{R}^3$ is a zero-mean Gaussian white noise vector, and $\xi_w \in \mathbb{R}^6$. The system matrix $A_w \in \mathbb{R}^{6 \times 3}$, the disturbance matrix $E_w \in \mathbb{R}^{6 \times 3}$ and the measurement matrix $C_w \in \mathbb{R}^{3 \times 6}$ may formulated as

$$A_w = \begin{bmatrix} 0_{3 \times 3} & I_{3 \times 3} \\ -\Omega^2 & -2\Lambda\Omega \end{bmatrix}, \quad (7a)$$

$$C_w = [0_{3 \times 3} \quad I_{3 \times 3}], \quad E_w = \begin{bmatrix} 0_{3 \times 3} \\ K_w \end{bmatrix}, \quad (7b)$$

where $\Omega = \text{diag}(\omega_1, \omega_2, \omega_3)$, $\Lambda = \text{diag}(\zeta_1, \zeta_2, \zeta_3)$ and $K_w = \text{diag}(K_{w1}, K_{w2}, K_{w3})$.

From a practical point of view, the WF model parameters are slowly-varying quantities depending on the prevailing sea state. Typically, the wave periods T_i , corresponding to wave frequency $\omega_i = 2\pi/T_i$, are in the range of 5 to 20 seconds in the North Sea for wind generated seas. The periods of swell components may be even longer than 20 seconds. The relative damping ratio ζ_i will typically be in the range 0.05 – 0.10.

Given the values for T_i , ζ_i , and K_w , we can construct the matrices A_w , C_w , and E_w . In our simulation, we set $T_i = [9, 9, 9]$, $\zeta_i = [0.05, 0.05, 0.05]$ and $K_w = [1, 1, 1]$. Then,

$$A_w = \begin{bmatrix} 0 & 0 & 0 & 1.0000 & 0 & 0 \\ 0 & 0 & 0 & 0 & 1.0000 & 0 \\ 0 & 0 & 0 & 0 & 0 & 1.0000 \\ -0.4874 & 0 & 0 & -0.0698 & 0 & 0 \\ 0 & -0.4874 & 0 & 0 & -0.0698 & 0 \\ 0 & 0 & -0.4874 & 0 & 0 & -0.0698 \end{bmatrix}$$

$$C_w = \begin{bmatrix} 0 & 0 & 0 & 1 & 0 & 0 \\ 0 & 0 & 0 & 0 & 1 & 0 \\ 0 & 0 & 0 & 0 & 0 & 1 \end{bmatrix}$$

$$E_w = \begin{bmatrix} 0 & 0 & 0 \\ 0 & 0 & 0 \\ 0 & 0 & 0 \\ 1 & 0 & 0 \\ 0 & 1 & 0 \\ 0 & 0 & 1 \end{bmatrix}$$

3.3 Bias model

There are two common used bias models in marine applications, which are first-order markov process and wiener process. In this project, we used first-order markov process. The bias model can be written as follows:

$$\dot{\mathbf{b}} = -T_b^{-1}\mathbf{b} + E_b \mathbf{w}_b, \quad (8)$$

where $\mathbf{w}_b \in \mathbb{R}^3$ is a zero-mean Gaussian white noise vector, $T_b \in \mathbb{R}^{3 \times 3}$ is a diagonal matrix of bias time constants, and $E_b \in \mathbb{R}^{3 \times 3}$ is a diagonal scaling matrix. We choose $T_b = \text{daig}([60, 60, 60])$ and $E_b = \text{eye}(3)$

The bias model accounts for slowly-varying forces and moment due to 2nd-order wave loads, ocean currents and wind. In addition, the bias model will account for errors in the modeling.

3.4 Measurement model

The measurement model is written as follows:

$$\mathbf{y} = \boldsymbol{\eta} + C_w \boldsymbol{\xi} + \mathbf{v}, \quad (9)$$

where $\mathbf{v} \in \mathbb{R}^3$ is the zero-mean Gaussian measurement noise vector.

3.5 Complete control plant model

The resulting control plant model is written

$$\dot{\boldsymbol{\xi}} = A_{\boldsymbol{\xi}} \boldsymbol{\xi} + E_w \mathbf{w}_w, \quad (10a)$$

$$\dot{\boldsymbol{\eta}} = R(\psi) \boldsymbol{\nu}, \quad (10b)$$

$$\dot{\mathbf{b}} = -T_b^{-1} \mathbf{b} + E_b \mathbf{w}_b, \quad (10c)$$

$$M \dot{\boldsymbol{\nu}} = -D \boldsymbol{\nu} - R^T(\psi) G \boldsymbol{\eta} + R^T(\psi) \mathbf{b} + \boldsymbol{\tau}, \quad (10d)$$

$$\mathbf{y} = \boldsymbol{\eta} + C_w \boldsymbol{\xi} + \mathbf{v}. \quad (10e)$$

4 Wind Model

Wind is a significant factor in the consideration of environmental loads and is characterized by two main parameters: velocity (U) and direction (ψ). The wind model can be broken down into three key components: a mean component, a slowly varying component, and a gust component.

4.1 Implementation

Just like the current, wind is defined in the NED frame, with only the North and East components being active. The mean wind velocity \bar{U} at height z can be expressed as:

$$\bar{U}(z) = \bar{U}_{10} \frac{5}{2} \sqrt{k} \ln\left(\frac{z}{10e^{-\frac{2}{5\sqrt{k}}}}\right) \quad (11)$$

The slowly varying component in the mean wind velocity can be represented by a Gauss-Markov process,

$$\dot{U}_{sv}(z) + \mu U_{sv} = w \quad (12)$$

The gust component is calculated using the Norsok (2018) wave spectrum and is then added together with the two other components to create the wind velocity V_w . The direction of the wind also has a slow varying component and mean component but not a gust component. The angle variation is limited to a maximum of 5 degrees around the mean direction. It is then used with the heading of the vehicle to determine the relative angle α_{rw} which makes it possible to find the wind coefficients in the coefficient matrix $C_w(x)$. We got the model of the wind force for calculation:

$$F_{Wind} = |V_w|^2 \cdot C_w(\alpha_{rw}) \quad (13)$$

The force calculation is executed within Simulink, utilizing a MATLAB function block to select the appropriate coefficients and compute the corresponding forces. The comprehensive Simulink representation of the wind can be found in the Figure.

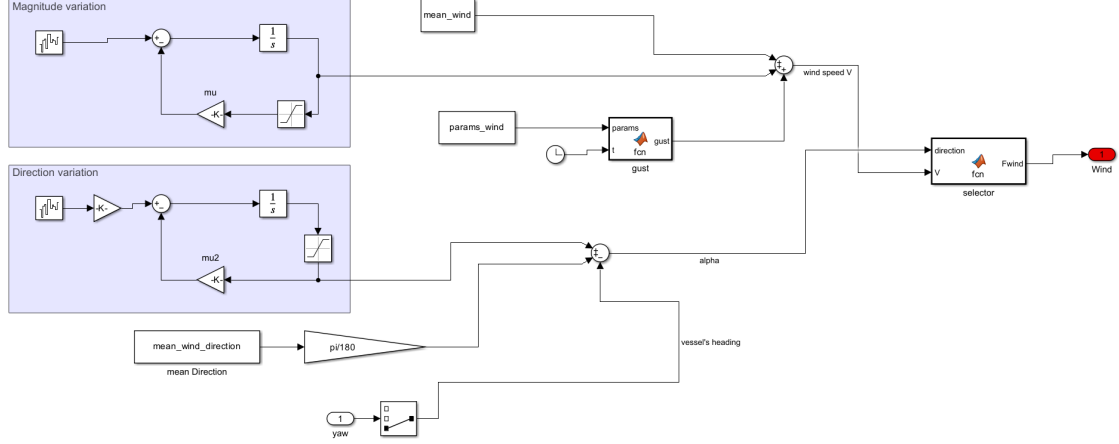


Figure 2: implementation of wind model with variation in magnitude and direction.

5 Wave Model

The ship's response to waves is simulated using two blocks from the MSS Toolbox. The initial block computes harmonic wave component parameters, offering flexibility with options such as ITTC, Jonswap, Torsethaugen, or predefined wave spectra. Parameters like significant wave height, peak frequency, mean wave direction, etc., can be conveniently specified within the Simulink block. The second block utilizes both wave component parameters and ship states (η) to determine wave loads (τ_{wave}). The schematic representation of these blocks is depicted in the figure 3.

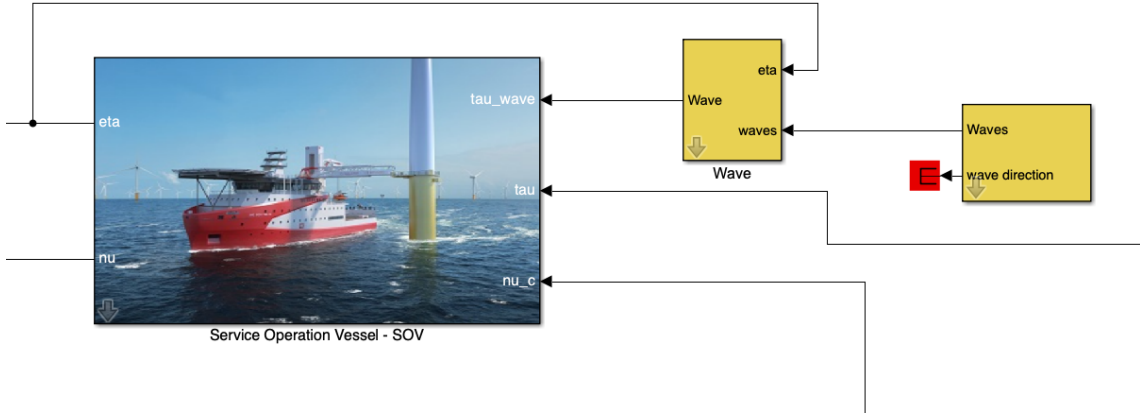


Figure 3: Wave Model

6 Current model

For surface vessel modeling, a 2D current model is enough and the down component is neglected. If V_c is the current magnitude and ψ_c is the direction in the NED frame, the current velocity vector \mathbf{v}_c is given by

$$\mathbf{v}_c = [V_c \cos(\psi_c), V_c \sin(\psi_c), 0]^T. \quad (14)$$

The variation in current velocity is described by a 1st order Gauss-Markov Process (Fossen, 2011):

$$\dot{V}_c + \mu V_c = w \quad (15)$$

where w is Gaussian white noise and $\mu \geq 0$ is a constant. For $\mu = 0$, this represents a random walk process.

The magnitude of the velocity is constrained by saturation limits:

$$V_{c,\min} \leq V_c \leq V_{c,\max} \quad (16)$$

Similarly, the variation in current direction is implemented as follows:

$$\dot{\psi}_c + \mu^2 \psi_c = w_2 \quad (17)$$

with limits on ψ_c defined as:

$$\psi_{c,\min} \leq \psi_c \leq \psi_{c,\max} \quad (18)$$

Figure 4 shows the implementation of the current model in Simulink as the variation in magnitude is modeled as 1st order Gauss-Markov Process and then the variation is added to the mean value of the current. The same model is used for the direction of the current. For testing we set the noise power w and w_2 to zero so there is no variation.

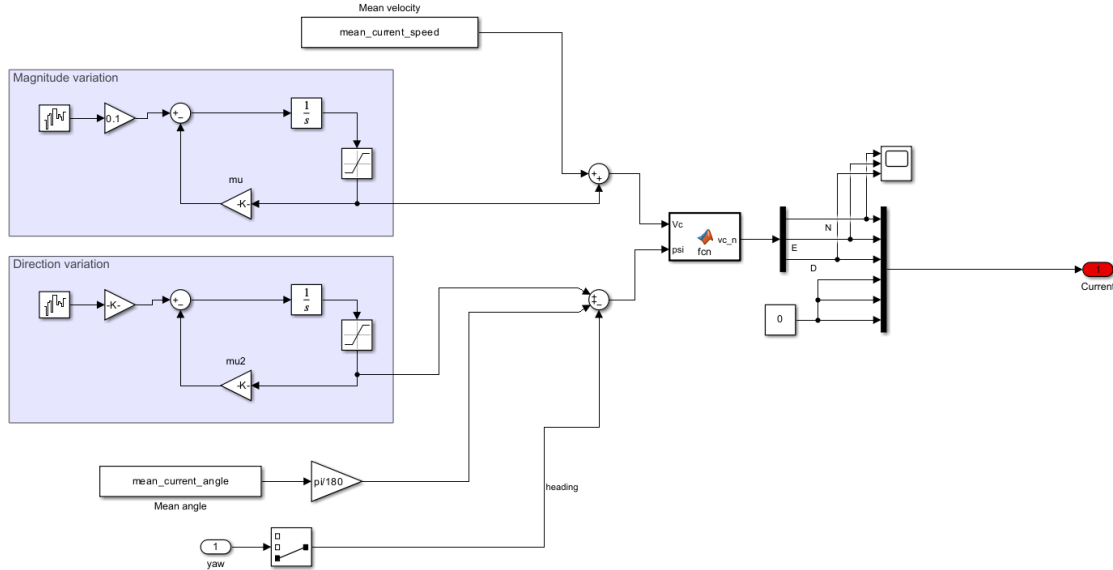


Figure 4: Implementation of current model with variation in magnitude and direction.

7 Reference Model

Dynamic Positioning (DP) operations require precision and reliability, especially when faced with changes in set points, known as the "marked position", or when the vessel is tasked with following a specific trajectory. To meet these demands, we employ a robust reference model. This model is designed not only to achieve the desired position, velocity, and acceleration based on predefined setpoints but also to respect the vessel's physical limitations, such as its maximum achievable speed and acceleration. In this section, we will explore the design of our reference model and the tuning values that ensure its optimal performance.

7.1 Mathematical Model

The reference model is governed by the following mathematical formulations:

$$a_d^e + \Omega v_d^e + \Gamma x_d^e = \Gamma x_{ref} \quad (19)$$

$$\dot{x}_{ref} = -A_f x_{ref} + A_f \eta_r \quad (20)$$

In these equations, a_d^e, v_d^e , and $x_d^e \in \mathbb{R}^3$ represent the desired vessel acceleration, velocity, and position trajectories in the Earth-fixed frame. The vector η_r provides the new reference coordinates, which can be relative to the previous setpoint or global Earth-fixed coordinates. The x_{ref} vector $\in \mathbb{R}^3$ denotes the filtered reference coordinates. The model's design parameters encompass a non-negative diagonal damping matrix $\Omega \in \mathbb{R}^3$ and a diagonal stiffness matrix $\Gamma \in \mathbb{R}^3$:

$$\Omega = \text{diag}\{2\zeta_i \omega_i\}, \quad i = 1, 2, 3 \quad (21)$$

$$\Gamma = \text{diag}\{\omega_i^2\}, \quad i = 1, 2, 3 \quad (22)$$

The first-order diagonal and non-negative setpoint filter gain matrix A_f is defined as:

$$A_f = \text{diag}\{1/t_i\}, \quad i = 1, 2, 3 \quad (23)$$

The transformation from the NED frame to the reference frame is done in the controller.

7.2 Tuning Values

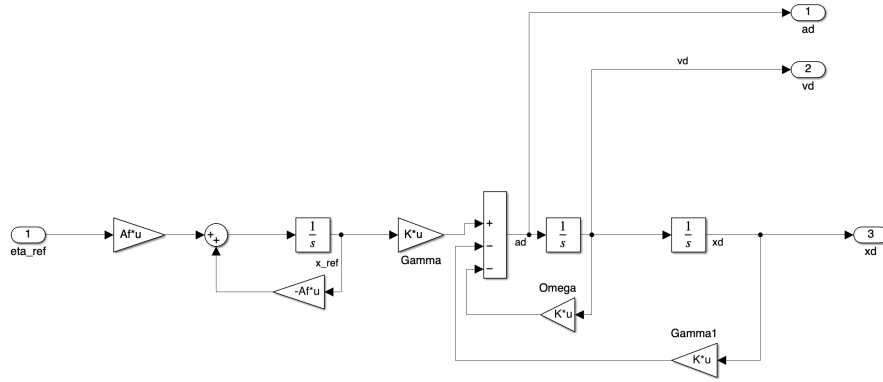
The reference model's parameters are:

$$\begin{aligned} t1 &= 10 \\ t2 &= 10 \\ t3 &= 20 \\ A_f &= \text{diag}\left(\frac{1}{t1}, \frac{1}{t2}, \frac{1}{t3}\right) \\ \omega &= [2\pi/100, 2\pi/100, 2\pi/50] \\ \zeta &= [0.9, 0.9, 1] \end{aligned}$$

These tuning values were meticulously chosen to achieve the desired position, velocity, and acceleration while adhering to the vessel's dynamic constraints, such as limited acceleration and velocity. Observations from plots confirmed that these constraints were not breached.

7.3 Simulink Diagram

Presented below is the Simulink diagram that visually represents the reference model:



W

Figure 5: Simulink representation of the reference model.

Also, we added a variable called "simulation" that takes values from 1 to 4 along with multi-switch blocks to select the simulation scenario as shown in figure 6.

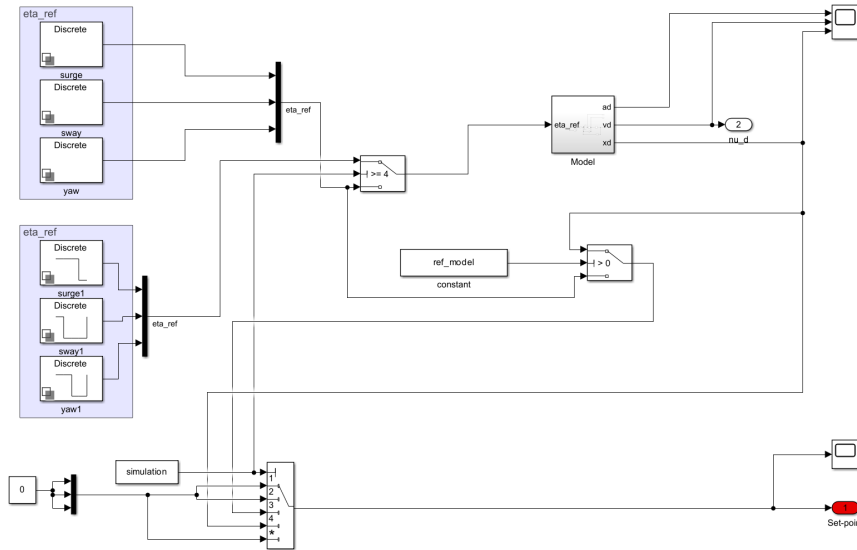


Figure 6: Simulink representation of the reference model with switching mechanism.

8 Observer design

We have implemented two observers that incorporate wave filtering, which are:

- Extended Kalman Filter (EKF)
- Non-linear Passive Observer

Each of these methods has its advantages and limitations.

EKF:

- EKF is more common to use and gives better accuracy if we can model the process and measurement noise

-
- EKF requires the computation of Jacobians at each time step due to model non-linearities. Driving the jacobian can be challenging in some cases, but in our case, it was straightforward
 - EKF might require a lot of tuning and it might require different tuning parameters depending on the operating point.

Non-linear Passive Observer:

- Non-linear Passive observer deals with the non-linear model without linearization as it required in EKF.
- It can be difficult to derive the equations of the non-linear passive observers
- It will require stability analysis
- It has less parameters to tune

The observer design is based on the complete control plant model ,as illustrated in eq(10), which consists of :

- Low-frequency control plant model
- Wave-frequency control plant model
- Bias model
- Measurements model

8.1 Extended Kalman Filter Design

The extended Kalman (EKF) filter design is based on the nonlinear model

$$\dot{x} = f(x) + Bu + Ew, \quad (24a)$$

$$y = Hx + v, \quad (24b)$$

where $f(x)$, B , E and H are given by

$$f(x) = \begin{bmatrix} A_w\xi \\ R(\psi)\nu \\ -T_b^{-1}b \\ -M^{-1}(-D\nu + R^T(\psi)b) \end{bmatrix}, \quad B = \begin{bmatrix} 0_{3x1} \\ 0_{3x1} \\ 0_{3x1} \\ M^{-1} \end{bmatrix},$$

$$E = \begin{bmatrix} E_w & 0_{3x3} \\ 0_{3x3} & E_b \end{bmatrix}, \quad H = [C_w \quad I_{3x3} \quad 0_{3x3} \quad 0_{3x3}],$$

Discrete-time EKF equations

The discrete-time EKF equations are given by:

Initial values:

$$\bar{x}_{k=0} = x_0, \quad (7.14a)$$

$$\bar{P}_{k=0} = \mathbb{E} [(x(0) - \hat{x}(0))(x(0) - \hat{x}(0))^T] = P_0 \quad (25)$$

Corrector:

$$K_k = P_{k|k-1}H^T[H\bar{P}_{k|k-1}H^T + R]^{-1}, \quad (26)$$

$$\hat{P}_k = (I - K_k H)\bar{P}_k(I - K_k H)^T + K_k R K_k^T, \quad (27)$$

$$\hat{x}_k = \bar{x}_k + K_k(y_k - H\bar{x}_k). \quad (28)$$

Predictor:

$$\bar{P}_{k+1} = \Phi_k \hat{P}_k \Phi_k^T + Q_k R_k Q_k^T, \quad (29)$$

$$\bar{x}_{k+1} = f(\hat{x}_k, u_k), \quad (30)$$

where $\hat{x}_k = [\hat{\xi}^T, \hat{\eta}^T, \hat{b}^T, \hat{\nu}^T]^T$, $f(\hat{x}_k, u_k)$, Φ_k , and R_k can be found by using *forward Euler* as follows:

$$f(\hat{x}, u) = \hat{x} + T[f(\hat{x}) + Bu], \quad (31)$$

$$\Phi_k = I_{n \times n} + T \frac{\partial f}{\partial x} \Big|_{\hat{x}_k, u_k}, \quad (32)$$

$$R_k = TE, \quad (33)$$

8.1.1 Implementation

The Extended Kalman Filter (EKF) is implemented as depicted in Figure 7. The discrete-time EKF equations are written inside the Matlab function. The Matlab function takes two inputs: y (measurement vector) and τ_{est} (estimated control input) and has two outputs: $\hat{\nu}$ and $\hat{\eta}$

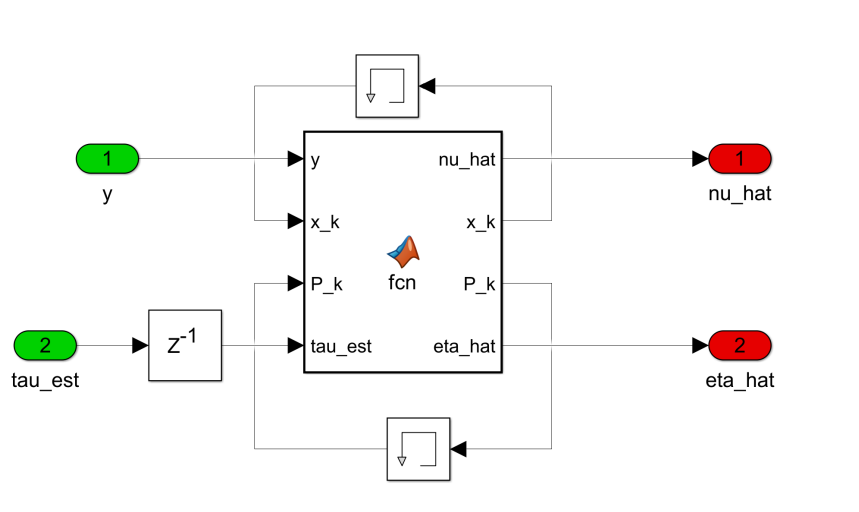


Figure 7: Schematic of the Extended Kalman Filter implementation.

8.1.2 Tuning values

For our system, we initialized the state vector x_0 and the covariance matrix P_0 as follows:

$$x_0 = \text{zeros}(15, 1),$$

$$P_0 = \text{diag}\left([1, 1, 1, \frac{\pi}{180}, \frac{\pi}{180}, \frac{\pi}{180}, 1, 1, \frac{\pi}{180}, 1 \times 10^5, 1 \times 10^5, 1 \times 10^5, 1, 1, \frac{\pi}{180}]\right).$$

For the process noise covariance matrix Q and the measurement noise covariance matrix R , we adopted a trial and error approach for tuning. These matrices are both diagonal, defined as:

$$Q = \text{diag}\left([1, 1, 0.01 \times \frac{\pi}{180}, 5 \times 10^4, 5 \times 10^4, 7 \times 10^5]^2\right),$$

$$R = \text{diag}\left([5, 5, 3 \times \frac{\pi}{180}]^2\right).$$

8.2 Non-linear Passive Observer

8.2.1 Observer Model Description

The observer is divided into two main models: the bias estimator on the left and the wave estimator on the right. The kinematics of the observer are captured by K_2 , which corresponds to the observer's velocity, while K_1 , K_3 , and K_4 are gain factors that modulate the influence of the observed errors on the state update.

The dynamics of the low-frequency motion are represented by the differential equations that describe the system's response to forces and moments, as shown in the equations for $\dot{\hat{v}}$ and \hat{y} , which correspond to the dynamics and measurement equations, respectively.

8.2.2 Observer Equations

The observer equations are given by:

$$\dot{\hat{\xi}} = A_w \hat{\xi} + K_y \tilde{y} \quad (34)$$

$$\dot{\hat{n}} = R(\psi) \dot{\hat{v}} + K_2 \tilde{y} \quad (35)$$

$$\dot{\hat{b}} = -T_b^{-1} \hat{b} + K_3 \tilde{y} \quad (36)$$

$$M \dot{\hat{v}} = -D(\hat{v}) \hat{v} + R^T(\psi) \hat{b} - G_{mo} R^T(\psi) K_4 \tilde{y} + \tau_c + R^T(\psi) K_d \tilde{y} \quad (37)$$

$$\hat{y} = \hat{n} + C_w \hat{\xi} \quad (38)$$

These equations represent the wave model, kinematics, bias, dynamics, and measurements of the observer system.

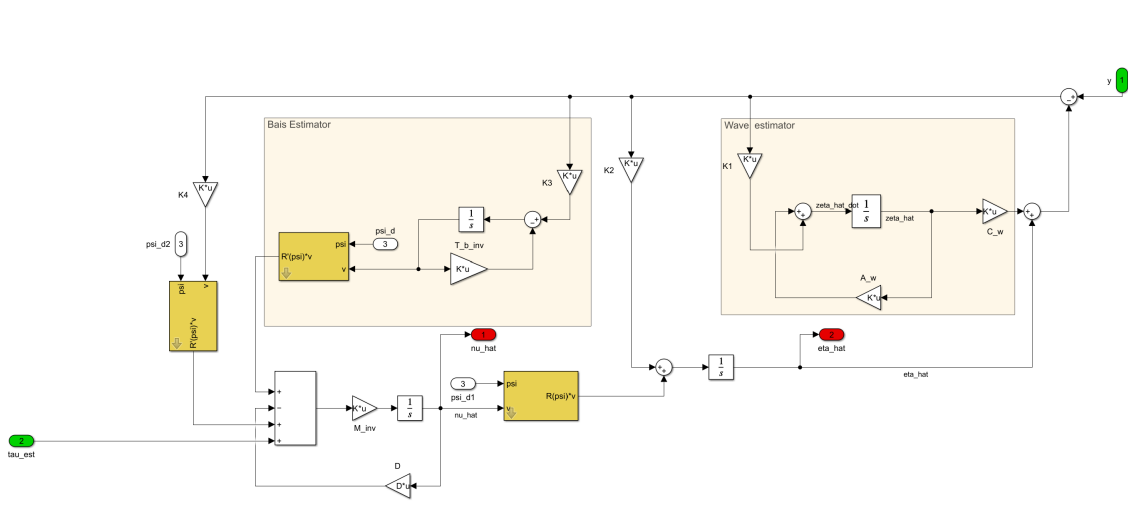


Figure 8: Non-linear Passive Observer, with the bias estimator model on the left, the wave estimator model on the right, K_2 representing kinematics, and the other components representing the dynamics of low-frequency motion.

8.3 Determination of the Observer Gains

The mapping H_2 describes three decoupled systems in surge, sway, and yaw. This suggests that the observer gain matrices should have a diagonal structure:

$$K_1(\omega_0) = \begin{bmatrix} \text{diag}\{K_{11}(\omega_{01}), K_{12}(\omega_{02}), K_{13}(\omega_{03})\} \\ \text{diag}\{K_{14}(\omega_{01}), K_{15}(\omega_{03}), K_{16}(\omega_{03})\} \end{bmatrix}$$

$$K_2 = \text{diag}\{K_{21}, K_{22}, K_{23}\}$$

$$K_3 = \text{diag}\{K_{31}, K_{32}, K_{33}\}$$

$$K_4 = \text{diag}\{K_{41}, K_{42}, K_{43}\}$$

These gain matrices are functions of wave frequencies in surge, sway, and yaw and open up possibilities for gain scheduling and an adaptive observer.

8.3.1 Observer Gain Tuning

The gains K_1 , K_2 , K_3 , and K_4 are tuned based on the wave response peak frequency, cutoff frequency, and other system parameters.

```
%choosing K1, K2, K3, and K4
T_peak = 9; % wave peak time period
omega_wave_i = 2*pi/T_peak; % wave peak frequency
omega_wave_c = 1.3 * omega_wave_i;
zeta_ni = 1;
zeta_n = 0.1;
% K1 parameters
k_1_3 = -2 * (zeta_ni - zeta_n) * (omega_wave_c/omega_wave_i);
k1 = k_1_3; k2 = k_1_3; k3 = k_1_3;
k_4_6 = 2 * omega_wave_i * (zeta_ni - zeta_n);
k4 = k_4_6; k5 = k_4_6; k6 = k_4_6;
% K2 parameters
k_7_9 = omega_wave_c;
k7 = k_7_9; k8 = k_7_9; k9 = k_7_9;
% choose K4 in order of magnitude of Mass matrix
k13 = 7.0101e6; k14 = 8.5190e6; k15 = 3.7973e9;
% choose K3 less than 0.1*K4. K3 = 0.01 * K4
K1 =[diag([k1, k2, k3]);
      diag([k4, k5, k6])];
K2 = diag([k7, k8, k9]);
K4 = diag([k13, k14, k15]);
K3 = 0.01 * K4;
```

Listing 1: MATLAB Code for Observer Gains

9 Thrust Allocation

9.1 Thrust Allocation Overview

Thrust allocation is essential in controlling marine vessels. It ensures the appropriate distribution of thrust among various thrusters to attain the desired motion.

9.1.1 Mathematical Model

For thrust allocation, the following equation is employed:

$$\tau_c = BU \quad (39)$$

Here, B is the actuator configuration matrix:

$$B(\alpha) = [t_1, t_2, t_3, t_4, t_5] \quad (40)$$

The three types of thrusters we utilize are:

- Tunnel thruster
- Azimuth thruster
- Main propeller

For the tunnel thruster:

$$t_i = \begin{bmatrix} 0 \\ 1 \\ x_i \end{bmatrix}$$

For the azimuth thruster:

$$t_i = \begin{bmatrix} \cos \theta_i \\ \sin \theta_i \\ \sin \theta_i \times x_i - \cos \theta_i \times y_i \end{bmatrix}$$

For the main propeller:

$$t_i = \begin{bmatrix} 1 \\ 0 \\ -y_i \end{bmatrix}$$

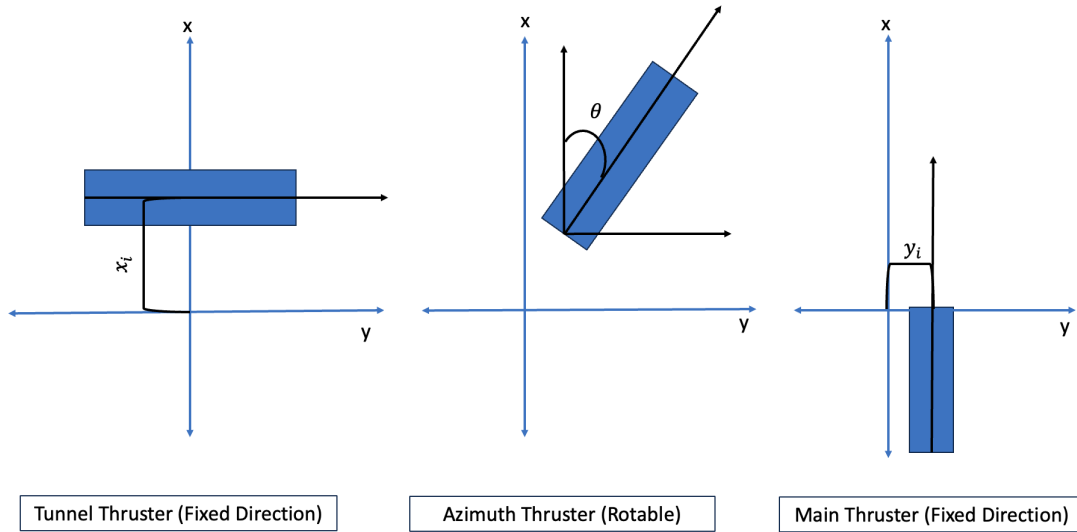


Figure 9: Illustration of the three types of thrusters.

9.2 Methods used

In our project, for the thrust allocation we implemented two methods: Pseudoinverse and Quadratic Programming. Then, We compared the efficiency of the two methods.

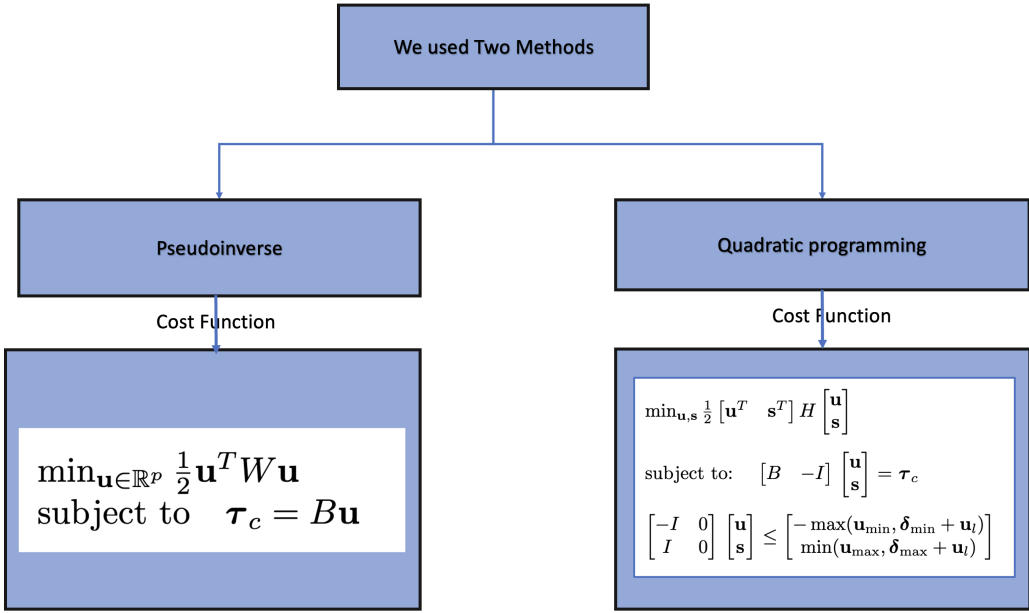


Figure 10: Thrust allocation methods used.

9.3 Optimization Process for Pseudoinverse vs. Quadratic Programming

The aim of the Pseudoinverse is to minimize energy consumption while ensuring the generation of the required force and torque. The unconstrained linear control algorithm is as follows:

$$\text{Pseudoinverse: Minimize } \frac{1}{2} \mathbf{U}^T W \mathbf{U}, \text{ subject to } \boldsymbol{\tau}_c = B \mathbf{U} \quad (41)$$

Where W is the weighting matrix. Choosing $W = I$ means equal usage for all thrusters. The control input \mathbf{U} can be calculated as:

$$\mathbf{U} = C \boldsymbol{\tau}_c$$

However, as matrix B isn't square, C isn't an exact inverse:

$$C = W^{-1} B^T (B W^{-1} B^T)^{-1}$$

In contrast, the Quadratic Programming method incorporates constraints directly into the optimization process, with a cost function that accounts for both control inputs and system states:

$$\text{Quadratic Programming: Minimize } \frac{1}{2} [\mathbf{u}^T \ \mathbf{s}^T]^T H \begin{bmatrix} \mathbf{u} \\ \mathbf{s} \end{bmatrix} \quad (42)$$

subject to

$$B \mathbf{u} = \boldsymbol{\tau}_c + \mathbf{s}, \quad (43)$$

$$\mathbf{u}_{\min} \leq \mathbf{u} \leq \mathbf{u}_{\max}, \quad (44)$$

$$\delta_{\min} \leq \mathbf{u} - \mathbf{u}_{\text{prev}} \leq \delta_{\max}. \quad (45)$$

9.3.1 Constraints

The thrust allocation algorithms, both Pseudoinverse and Quadratic Programming, must adhere to a set of inherent constraints to ensure operational integrity and safety:

- Maximum thrust (saturation)
- Rate limitations
- Forbidden sectors
- Power blackout/overload

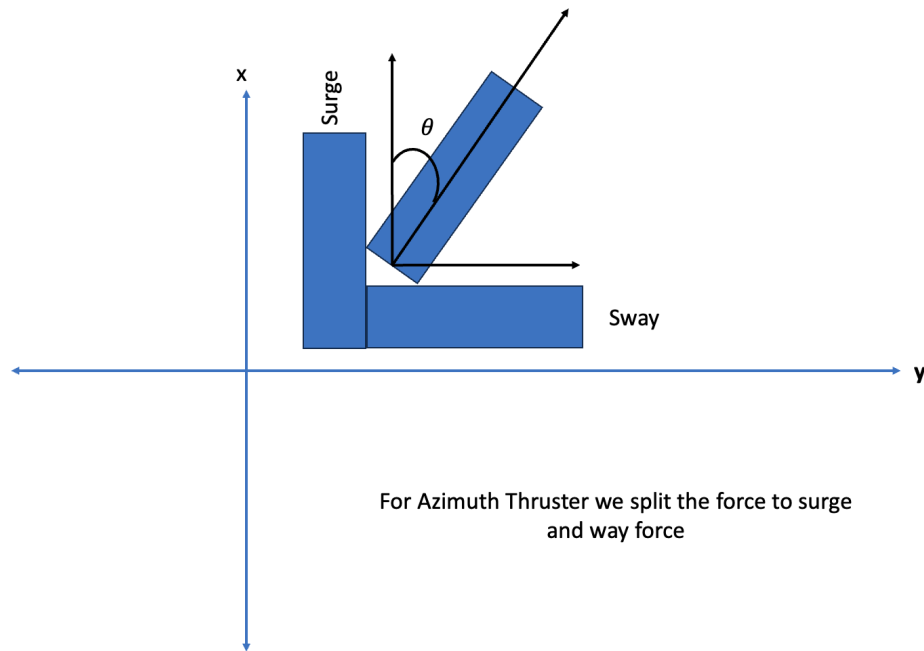


Figure 11: Dividing the azimuth force into x and y components.

Extended B Matrix We divided the Azimuth thruster into two vectors in surge and sway. so we got the 8 by 3 matrix.

$$B_e x = \begin{bmatrix} 0 & 1 & 0 & 0 & 1 & 0 & 1 & 0 \\ 1 & 0 & 1 & 1 & 0 & 1 & 0 & 1 \\ x_1 & -y_2 & x_2 & x_3 & -y_4 & x_4 & -y_5 & x_5 \end{bmatrix}$$

Thrust Allocation Implementations

We implemented two MATLAB functions for the thrust allocation: one employing a Pseudoinverse method and the other using Quadratic Programming.

Pseudoinverse Method

Our Pseudoinverse approach follows these steps:

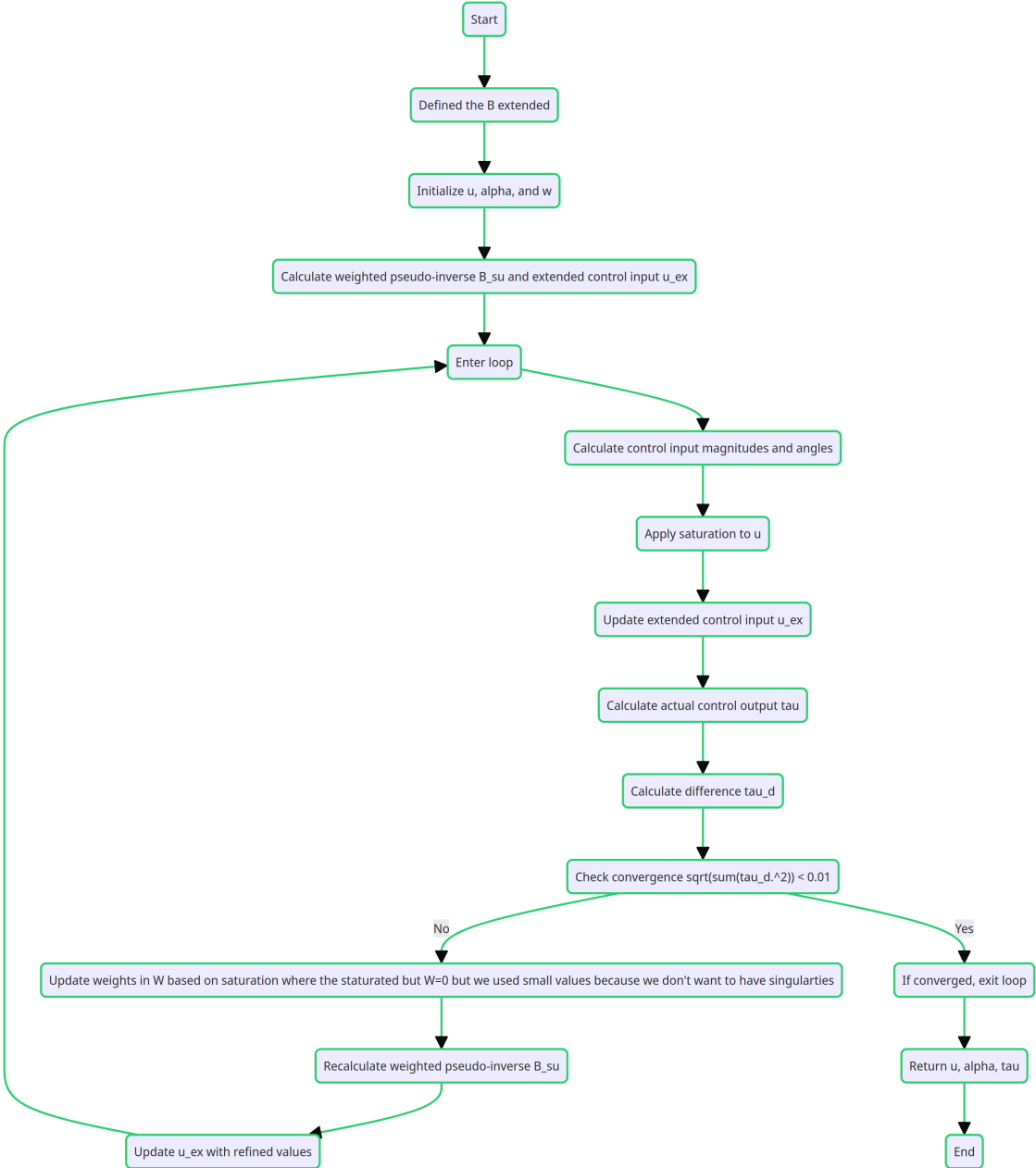


Figure 12: Our Matlab Algoirthm for Thrust allocation using the Pseudoinverse method.

Quadratic Programming Method

We formulated the QP thruster allocation problem in eq (42) with constraints to be use MATLAB's `quadprog` function to solve the optimization problem. One significant limitation of the `quadprog` function pertains to its inability to directly incorporate quadratic constraints for the maximum thrust of azimuth thrusters. This limitation necessitates a simplification in the approach to defining thrust constraints.

- We acknowledge that `quadprog` is primarily designed for linear or quadratic programming problems and does not natively support non-linear constraints, such as those needed for complex thruster dynamics.
- To address this limitation and simplify our model, we chose to equate the maximum horizontal and vertical components of the thrust.

- Specifically, we set both the horizontal and vertical components to be equal to half of the maximum thrust capacity of the azimuth thrusters.

```

function [u, alpha, u_opt]= fcn(tau_c, u_prev, xi, sample_time,
    ↪ thrust_max, thrust_rate, yi)
u = zeros(5,1);
alpha = zeros(5,1);
% Define the H matrix
p = 8; % number of u elements
m = 3; % number of s elements
W = eye(1,p);
Q = 1e4 * eye(1,m);
H = 2 * diag([W, Q]);

% Define the B matrix
B = [0, 1, 0, 0, 1, 0, 1, 0;
      1, 0, 1, 1, 0, 1, 0, 1;
      xi(1), 0, xi(2), xi(3), -yi(4), xi(4), -yi(5), xi(5)];

% Define equality constraint
Aeq = [B, -eye(m)];
beq = tau_c;

u_max = [thrust_max(1), thrust_max(2)/2, thrust_max(2)/2,
    ↪ thrust_max(3),
    thrust_max(4)/2, thrust_max(4)/2, thrust_max(5)/2,
    ↪ thrust_max(5)/2];
u_min = -u_max;

% Define inequality constraints
delta_max = [thrust_rate(1), thrust_rate(2), thrust_rate(2),
    ↪ thrust_rate(3),
    thrust_rate(4), thrust_rate(4), thrust_rate(5),
    ↪ thrust_rate(5)]' * sample_time;
delta_min = -delta_max;
Aineq = [-eye(p), zeros(p, m);
          eye(p), zeros(p, m)];
bineq = [-max(u_min, delta_min + u_prev);
          min(u_max, delta_max + u_prev)];

options = optimoptions('quadprog', 'Algorithm', 'active-set',
    ↪ 'Display', 'off',
    'StepTolerance', 1e-30, 'OptimalityTolerance'
    ↪ , 1e+1);
x0 = zeros(p+m,1);

% Call the quadprog function with the 'active-set' algorithm
u_s_opt = quadprog(H, [], Aineq, bineq, Aeq, beq, lb, ub, x0,
    ↪ options);

% Extract u
u_opt = u_s_opt(1:p);
u(1) = u_opt(1);
u(2) = sqrt(u_opt(2)^2 + u_opt(3)^2);
u(3) = u_opt(4);
u(4) = sqrt(u_opt(5)^2 + u_opt(6)^2);
u(5) = sqrt(u_opt(7)^2 + u_opt(8)^2);

```

```

alpha(1) = pi/2;
alpha(2) = atan2(u_opt(3), u_opt(2));
alpha(3) = pi/2;
alpha(4) = atan2(u_opt(6), u_opt(5));
alpha(5) = atan2(u_opt(8), u_opt(7));

```

Listing 2: MATLAB Code for Quadprog Optimization

10 Controller design

In this section, the controller will be selected, designed and tuned. From a pool of controllers available, the PID controller is preferred in this work for many reasons. Controllers, in general, are mathematical expressions that are introduced to the plant model to get a desired dynamics (i.e. stable). The main problem that we face in real-life applications is that, mostly, we don't have accurate model of the process/system of interest, especially in maritime applications where the environmental disturbances can be really hard to model. Moreover, vessels and floating platforms are inherently complicated and modeling of such systems can be very hard. This makes controllers like LQR and MPC, in spite of their strengths and predictive capabilities, risky to rely on in such applications. The added mathematical complexities in those controllers make it a difficult task to implement and troubleshoot trace back problems when they happen. On the other hand, PID controllers are more robust, and easy to apply and tune since they are defined within a very simple and intuitive mathematical framework. Moreover, there are large body of research and methods for tuning the PID controllers unlike the case of LQG and MPC. For instance, models available, even if inaccurate, can serve initializing the tuning process and fine tuning can be carried out after. Model insufficiency and environmental complex disturbances modeling can be overcome by putting the system in its operating conditions (i.e. putting the vessel at sea/pool) and fine tuning the DP system to account for these errors in the model. This makes PID a preferred choice by technology providers to adopt. This, consequently, makes us willing to learn how to design and tune this kind of controllers.

The mathematical model of PID controllers comes in three blocks as follows:

$$\tau_{\text{PID}} = K_p e(t) + k_d \frac{de(t)}{dt} + K_I \int e(t) dt \quad (46)$$

where:

- **Proportional controller** which simply gives control action depending on the error $e(t)$. If the error in the state is high, the control action is high as well, and if it's 0, there will be no control action. Moreover, it provides a direction for the system which is inherited from the sign of the error signal $e(t)$. If the system is behind the set point, the error will be positive and the control action will be positive, while if the system overshoots the set point, the error will be negative pulling back the control action in reverse direction. The parameter k_p is for tuning.
- **Integral controller** which learns from all past errors (bias in the model) and provides a correction signal which is crucial. It learns all the past errors by calculating the integral $\int e(t) dt$ while the parameter K_I is a tuning gain.
- **Derivative controller** which helps anticipating the future by taking the derivative of the error $\frac{de(t)}{dt}$ (slope of the error $e(t)$ curve) and giving control actions based on this information. While the derivative controller helps smoothing the system response, reduce oscillations, and make it more robust, it can be a problem if the error signal is not smooth (includes lots of ripples due to sensor noise). So, applying this controller requires further considerations and using proper filtering techniques to mitigate this issue. Similarly, the parameter K_D is tuning gain.

However, the resulted control action τ_{PID} is applied in the body frame, while the error $e(t)$ is measured in the NED frame. So, rotation matrix is introduced in the equation as follows:

$$\tau_{\text{PID}} = -K_p R^T(\psi) e(t) - k_d \tilde{\nu} - K_I R^T(\psi) \int e(t) dt \quad (47)$$

where:

- $e(t) = \eta - \eta_d$ (current state - desired state) in the NED frame
- $\tilde{\nu}$ (current velocity - desired velocity) in the body frame

It's also noticed that the velocity ($\tilde{\nu}$) is measured in the body frame by using the derivative block in SIMULINK to differentiate the transformed error ($R^T(\psi)e(t)$)

10.1 Tuning of the PID controller

We use the control plant model in Equation (5), and τ represents the control input from the PID controller, so we rewrite it as τ_{PID} . The control plant model is expressed as:

$$\mathbf{M}\dot{\nu} + \mathbf{D}\nu = \tau_{\text{PID}} \quad (48)$$

Let's set $\eta_d = 0$ and $\nu_d = 0$, which represent the desired position in NED frame and velocity in the body frame, respectively. We can rewrite equation 47 as follows:

$$\mathbf{M}\dot{\nu} + \mathbf{D}\nu = -K_p R^T(\psi)\eta - k_d \nu - K_I R^T(\psi) \int \eta dt \quad (49)$$

And further simplify it to:

$$\mathbf{M}\dot{\nu} + (D + K_d)\nu + K_p R^T \eta = -K_I R^T(\psi) \int \eta dt \quad (50)$$

Dividing by \mathbf{M} , we obtain:

$$\dot{\nu} + \frac{(D + K_d)}{M}\nu + \frac{K_p}{M} R^T \eta = -\frac{K_I}{M} R^T(\psi) \int \eta dt \quad (51)$$

Typically, the bandwidth of the DP system for a vessel is $T_n^{DP} = 50 - 200$ s, so we have:

$$(\omega_n^{DP})^2 = \frac{K_p}{M}, \quad \omega_n^{DP} = \frac{2\pi}{T_n^{DP}} \quad \therefore \quad K_p = M \left(\frac{2\pi}{T_n^{DP}} \right)^2 \quad (52)$$

Substituting $M = 6362208.5$ kg and $T_n^{DP} = 100$ s, we get $K_p = 2.5117 \times 10^4$.

K_I should be smaller than K_p . It is recommended in [1] to be:

$$K_I = \frac{\omega_n^{DP}}{10} K_p \quad \therefore \quad K_I = 157.8 \quad (53)$$

We choose the value of K_d such that the peak of τ_d is two-thirds of the peak of τ_p . Therefore, we set $K_d = 3 \times 10^4$.

Table 1: PID Controller Gains for Surge, Sway, and Yaw used in part 1

Motion	K_p	K_i	K_d
Surge	114000	1586	2030000
Sway	788000	23000	5950000
Yaw	78300000	1068000	763500000

We choose these values to initialize the PID controllers (for Surge, Sway, and Yaw), then fine-tuned K_p , K_d , and K_I through a process of trial and error to achieve a better response. Table 1 shows the fine tuned parameters used in simulation (part 1).

In Part 2 of our study, we integrated thruster dynamics into our system model and implemented a PID controller. The initial PID parameters, as detailed in Table 1, resulted in excessively high control inputs that exceeded the operational capabilities of the thrusters. To align the control inputs with the practical limitations of the thrusters, we undertook a recursive tuning process.

- We observed that the original PID gains led to desired torque values, denoted as τ_d , which were unattainable by our thrusters.
- To address this, we systematically adjusted the PID gains. This tuning was performed iteratively, employing a trial and error methodology.
- Our objective was to achieve reduced τ_d values, ensuring they remained within the feasible range of the thrusters' capabilities.

This refinement of the PID controller's gains was critical to ensure that the control inputs were both effective and realistic, given the physical constraints of our thrusters.

Table 2 shows the fine tuned parameters used in simulation (part 2).

Table 2: PID Controller Gains for Surge, Sway, and Yaw used in part 2

Motion	K_p	K_i	K_d
Surge	110700	2213	1233289
Sway	134500	2690	1498741
Yaw	59964412	1199288	668054281

11 Simulation Results

11.1 Part 1

As shown in the previous section, the controller has been tuned to get an acceptable response from the system. In this section, simulations are to be carried out and system response is discussed. To test and evaluate our system, 4 simulations are conducted to evaluate all different parts of the proposed solution (current model, reference model, and controller) as follows:

- **Simulation 1:** testing the DP system's capability to keep the vessel's pose under fixed current disturbance.
- **Simulation 2:** testing the DP system's capability to keep the vessel's pose under changing current disturbance.
- **Simulation 3:** testing the controller's performance with and without reference model to chase after desired set point. This will allow us to evaluate both, the controller and the reference model.

- **Simulation 4:** testing the system's capability to follow on and stay on a path of 5 states without disturbance. This will show the overall system's capability to carry out more complicated maneuvers.

11.1.1 Simulation 1

For the first simulation, show the DP capabilities of your DP system. With the DP setpoint set to [000] and current set to 0.5[m/s], going to southeast. Plot the position and heading until you reach steady state, both as individual results and in a xy – plot.

Since the target is to keep the vessel in place and orientation, the set-point will be always [000] and the reference model will not have any effect in this case. The vessel will be disturbed by sudden fixed magnitude and orientation current in the **South-East** direction. Thus:

$$V_c = 0.5 \text{ m/s}$$

$$\psi = 135^\circ$$

The following figures show the system response.

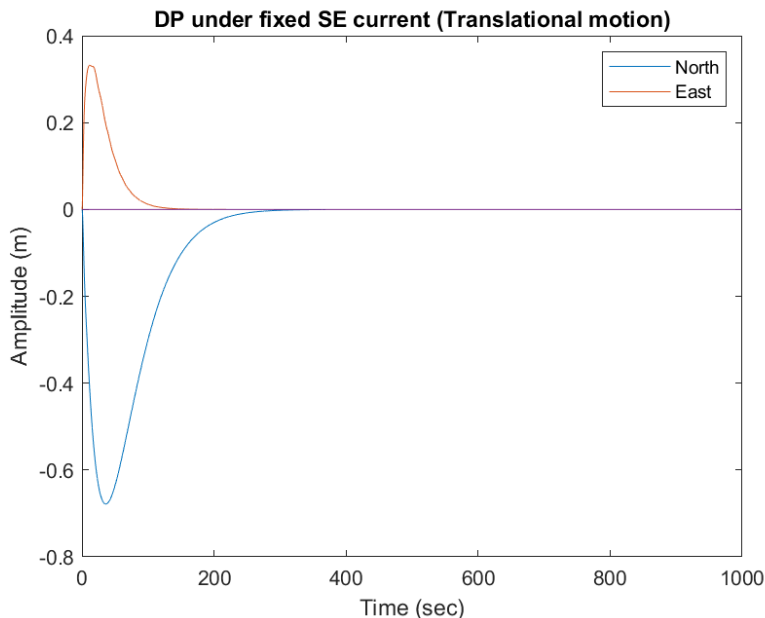


Figure 13: This figure represents the position of the vehicle in the NED frame when disturbed by fixed current of magnitude 0.5 m/s in the South-East direction. The red curve denotes the motion in East-axis, while the blue curve denotes the vehicle's motion in the North-axis.

Figure 13 shows the vehicle's motion in any direction is no more than 1m which reflects the efficiency of the system. Also, at first, the vehicle's is found to be obviously pushed from the [00] position to the South-East direction, since the blue curve is in the negative side (south) while the red curve is in positive side (East). This indicates a valid representation of the current through our current model. One important observation to note is that the peak displacement in the north direction is greater than the one in the east direction. This is because its easier to move the vessel in surge than in sway because of the damping forces. This proves that the mathematical model of the vessel is consistent.

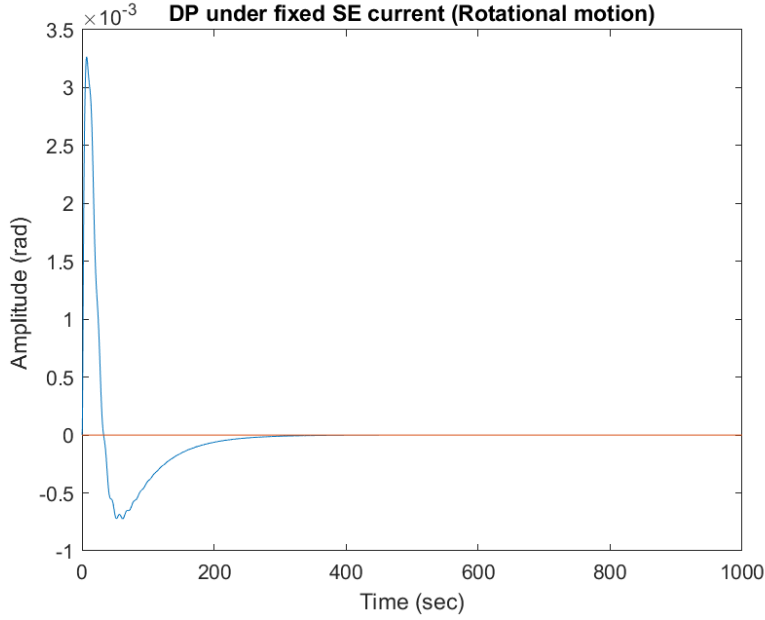


Figure 14: This figure represents the Orientation of the vehicle in the NED frame when disturbed by fixed current of magnitude $0.5m/s$ in the South-East direction

Figure 14 shows the change of the vessel's heading from north to more towards the east, as shown in the first spike. However, the heading drops again to 0 and overshoots. This shows the controller's effort to adjust the heading of the vehicle. This overshoot is acceptable since the magnitude is negligible.

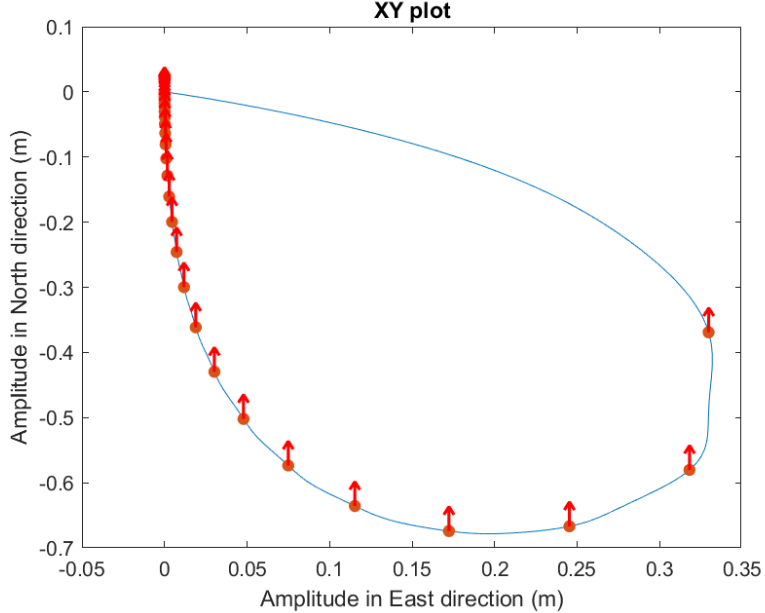


Figure 15: This figure represents a XY-plot the shows both position and heading of the vessel in the NED frame when disturbed by fixed current of magnitude $0.5m/s$ in the South-East direction. The North-East position is indicated by the blue curve, while the heading is represented by the red arrows. Heading samples is taken every 1000 measurements.

Figure 15 shows that the vessel didn't move for too much from the set point. Also, the whole curve lies in the South-East quarter, which proves the validity of the current model. As the heading is

plotted every 1000 measurements, we can deduct that the side with less arrows directly after the set point marks the beginning of the disturbance and the direction in which the vessel moves in the North-East plane.

11.1.2 Simulation 2

Now, make the current vary linearly from coming from North to 0.5[m/s] coming from East, while keeping the vessel at the origin [0,0,0]. Plot the position and heading until you reach steady state, both as individual results and in a xy-plot.

The target now is to test the performance of the DP under varying current direction and fixed magnitude. The varying current is modeled as follows:

- Coming from north to coming from east is equivalent to a change from 180° to 270°
- The change is modeled by a ramp with a slope of 1rad/sec , which means that the disturbance change orientation for 90sec and then saturates at 270° (west/ coming from east).

The following figures show the system response.

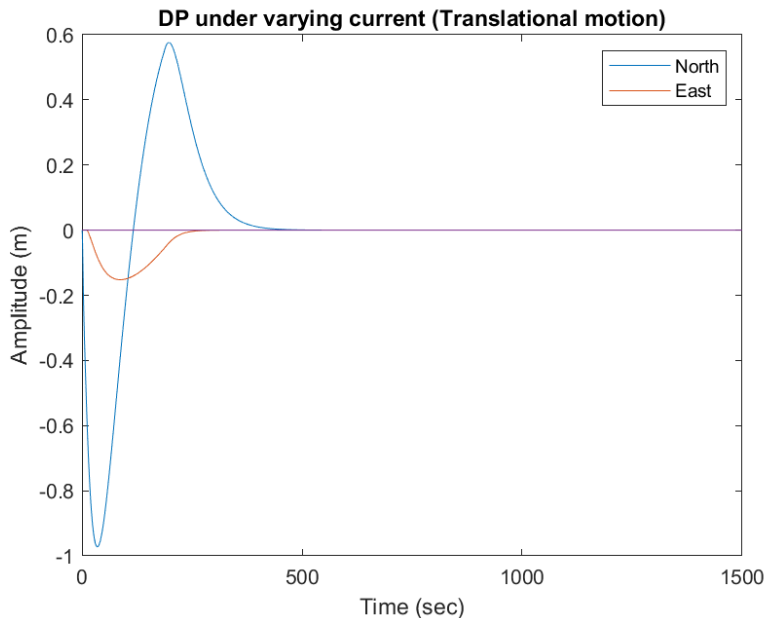


Figure 16: This figure represents the position of the vehicle in the NED frame when disturbed by fixed current of magnitude 0.5m/s and varying direction from south to west direction. The red curve denotes the motion in East-axis, while the blue curve denotes the vehicle's motion in the North-axis.

Figure 16 shows the vessel's motion in any direction is no more than 1m which reflects the efficiency of the system. The vessel is pushed first to the south, then, after few seconds, we can see the vessel is starting to move in the west direction. This delay is because at the first few seconds, the component of the current in the west direction is still small and cannot move the vessel, especially with large drag forces in the sway direction. This effect of changing direction is also present in the phase shift between peaks of vessel's motion in north or east directions. It's found that the peak of the blue curve is back to 0 near the time of 90sec , this may be because that the component of current in the south direction is slowly vanishing. Also, it's interesting to notice that the red curve is approaching 0m even though the current component is increasing overtime [from time of 100 sec to 180 sec]. This demonstrates basic predictive capability of the controller.

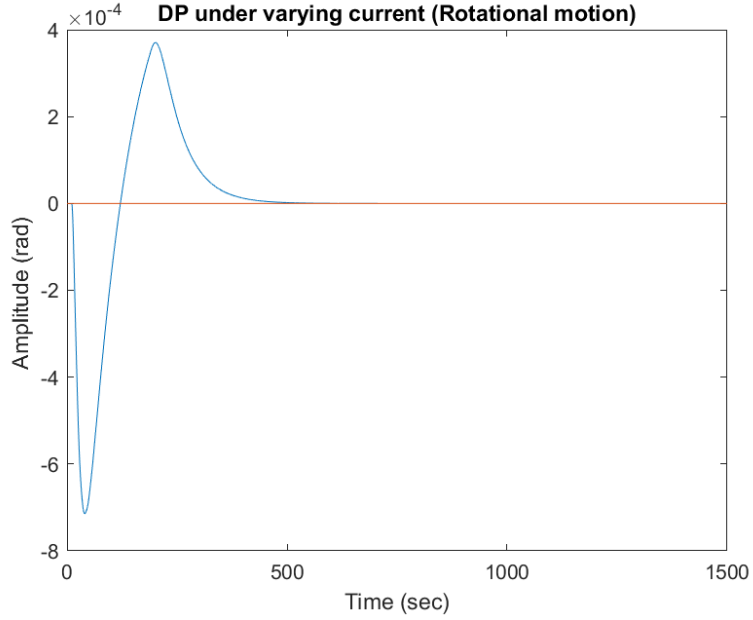


Figure 17: This figure represents the Orientation of the Vessel in the NED frame when disturbed by Varying current of fixed magnitude $0.5m/s$ and varying direction from south to west

Figure 17 shows the same lag discussed before, in the first few seconds. Then, there's a change of the vessel's heading from north to more towards the west, as shown in the first spike. However, the heading drops again to 0 and overshoots. This shows the controller's effort to adjust the heading of the vehicle. This overshoot is acceptable since the magnitude is negligible.

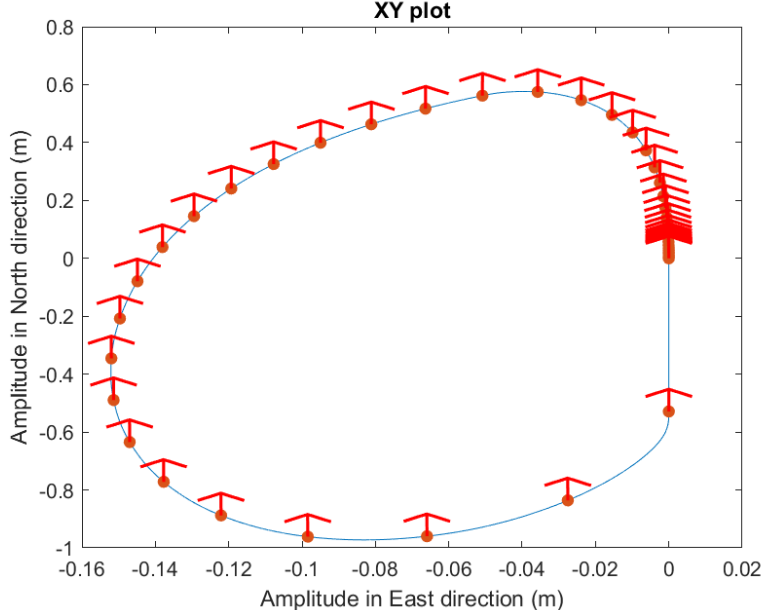


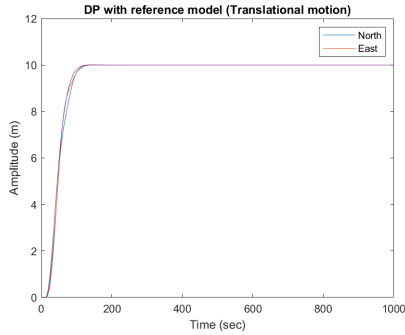
Figure 18: This figure represents a XY-plot the shows both position and heading of the vessel in the NED frame when disturbed by fixed current magnitude $0.5m/s$ and varying current direction. The North-East position is indicated by the blue curve, while the heading is represented by the red arrows. Heading samples is taken every 1000 measurements.

Figure 18 shows that the vessel didn't move for too much from the set point. Also, the whole curve lies in the western half of the plane, because the current is growing more in the west direction.

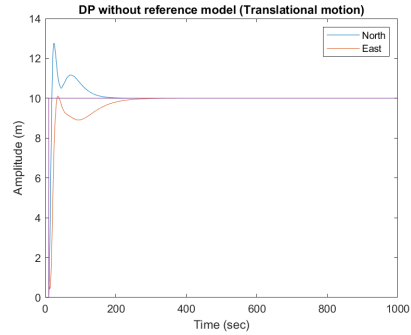
11.1.3 Simulation 3

Compare the different results for a vessel position over time for initial position $\eta_0 = [0, 0, 0]$ and $\eta_{SP} = [10, 10, 3\pi/2]$, with and without a reference model. Both simulations shall be performed without environmental forces. Plot the position and heading until you reach 4 steady state, both as individual and in a xy-plot. In addition, put the desired trajectory in the individual plots. If the reference model contains velocity trajectories, then plot these with the actual velocities.

Without environmental disturbance, the controller and the importance and efficacy of the reference model. The following figures show the system response.



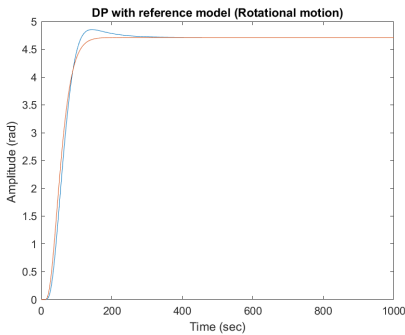
(a) Translation motion without reference model



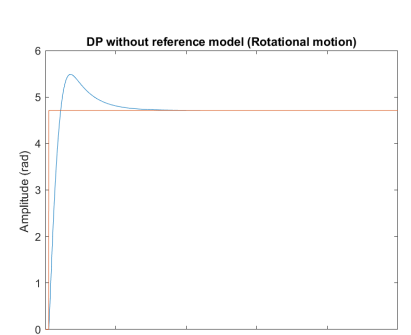
(b) Translation motion with reference model

Figure 19: This figure represents the DP performance in making the vehicle move from $\eta_0 = [0, 0]$ to $\eta_{SP} = [10, 10]$ with and without reference model.

Figure 19a shows the vessel's motion is very smooth and following the reference model almost without deviation. Almost no overshoot (negligible) and the settling time is below 200sec which is very good. unlike the case with 19b, the system overshoots drastically and the settling time is much higher. Also, the control effort sent to the actuators is expected to be very large (because the set point is far and consequently the error fed to the PID controller). This figure reflects the importance of using a smooth reference model.



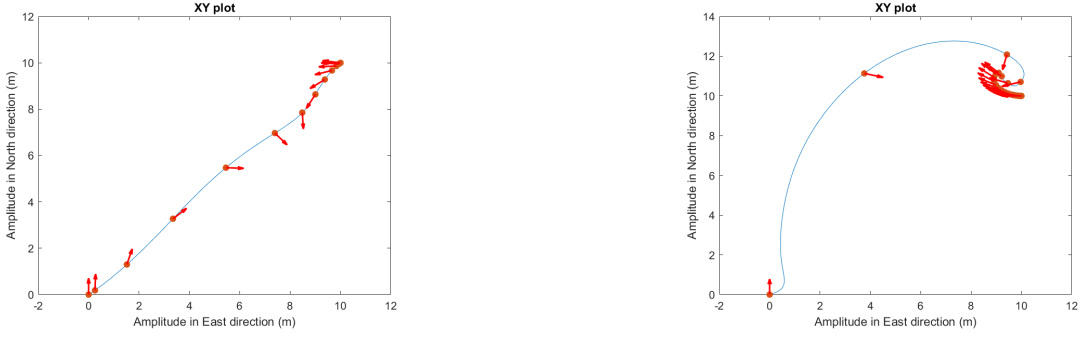
(a) Rotation motion without reference model



(b) Rotation motion with reference model

Figure 20: This figure represents the DP performance in making the vehicle change its heading from $\psi_0 = [0]$ to $\psi_{SP} = [3\pi/2]$ with and without reference model.

Figure 20a shows a smoother transition in heading if we use the reference model as expected. Although both systems overshoot, we clearly see the overshoot in 20a is far less than in figure 20b. This overshooting problem can be addressed by further tuning of the rotational motion reference model.



(a) motion in xy-plane without reference model

(b) motion in xy-plane with reference model

Figure 21: This figure represents the DP performance represented by xy-plot in making the vehicle change its state from $\psi_0 = [0, 0, 0]$ to $\psi_{SP} = [10, 10, 3\pi/2]$ with and without reference model. The Red arrows represent the vessels heading while the blue line represents the path in the xy-plane.

Figure 21a shows a very smooth transition to destination with almost straight path. Moreover, it's obvious to notice the transition of the heading along the path from 0° (pointing in the north) to 270° (pointing west) if we use the reference model. On the other hand, the transition in the state is wild in Figure 21b if we don't use the reference model. Moreover, because the controller is fine tuned, the gains are large. Hence, with large error (i.e. in the case of far set point without reference model), we find that, in simulation, the rise time is very short as in Figure 19b which is not realistic or even dangerous on the vessel. Even if the vessel could move in such high speed, this will cause a wear in the thrusters, and there must be a saturation level to the control signal to mitigate such problem.

11.1.4 Simulation 4

The last mandatory simulation is to perform a DP 4 corner test. Perform this simulation without environmental forces, and go through the following set-points ($\eta_0 = [0, 0, 0]$, $\eta_1 = [50, 0, 0]$, $\eta_2 = [50, -50, 0]$, $\eta_3 = [50, -50, -\pi/4]$, $\eta_4 = [0, -50, -\pi/4]$, $\eta_5 = [0, 0, 0]$)
The vessel must keep a steady position on the desired set-point before moving on to the next.

The previous simulations were enough to test the performance of individual blocks of the system (current model, reference model, and controller). The aim of this simulation is to test how these blocks can work together (reference model + controller blocks) to move the vehicle through set of desired states. From Simulation 3, we notice in figure 19a that the reference model needs about 200sec for the vehicle to settle in the final desired state. Thus, the provided 5 desired states of the system are encoded in SIMULINK with a period of 200sec allocated for each state during which the vessel should be stable at the desired state. The following figures show the system response.

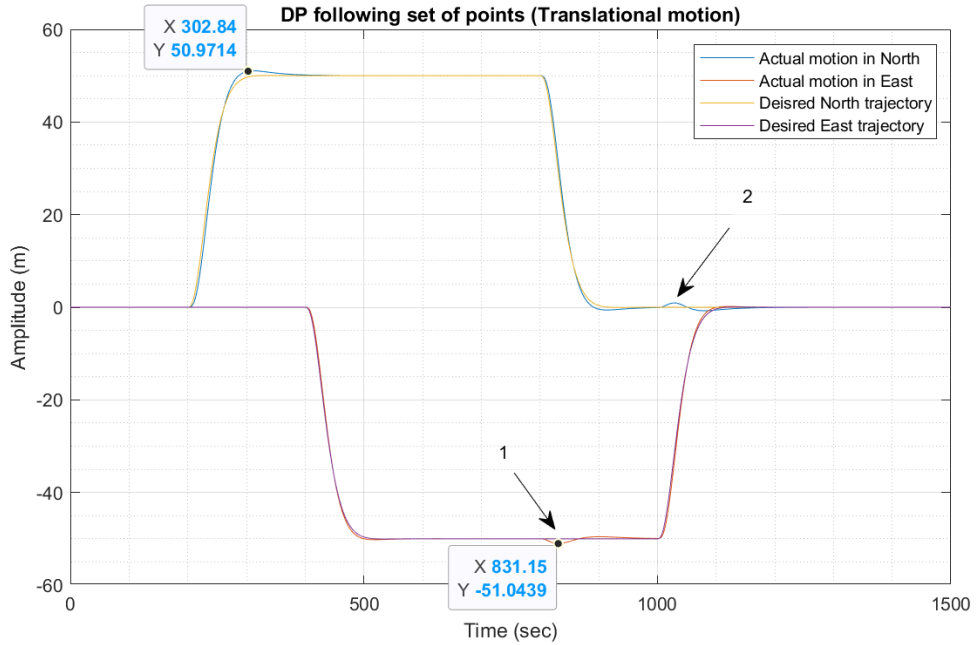


Figure 22: This figure represents the position of the vehicle in the NED frame following a set of desired points without any environmental disturbances. The red curve denotes the motion in East-axis, while the blue curve denotes the vehicle's motion in the North-axis. The text boxes provide information about maximum overshoot happening in the system's position, while the arrows are pointing at regions of interest to be discussed and explained.

From Figure 22, we notice that the system is following the desired states very smoothly with minimum overshoots as shown from the textboxes indicating marked at places with maximum overshoot happening in the system. They show a maximum overshoot no more than 1.5m which is very good. However, as the system is stable at the set point, a disturbance happens and the vessel needs to compensate again. The arrows are pointing at 2 locations where these kind of disturbances happen. To understand what's happening, we need to study the next curve (heading control) and also to go back to the desired states.

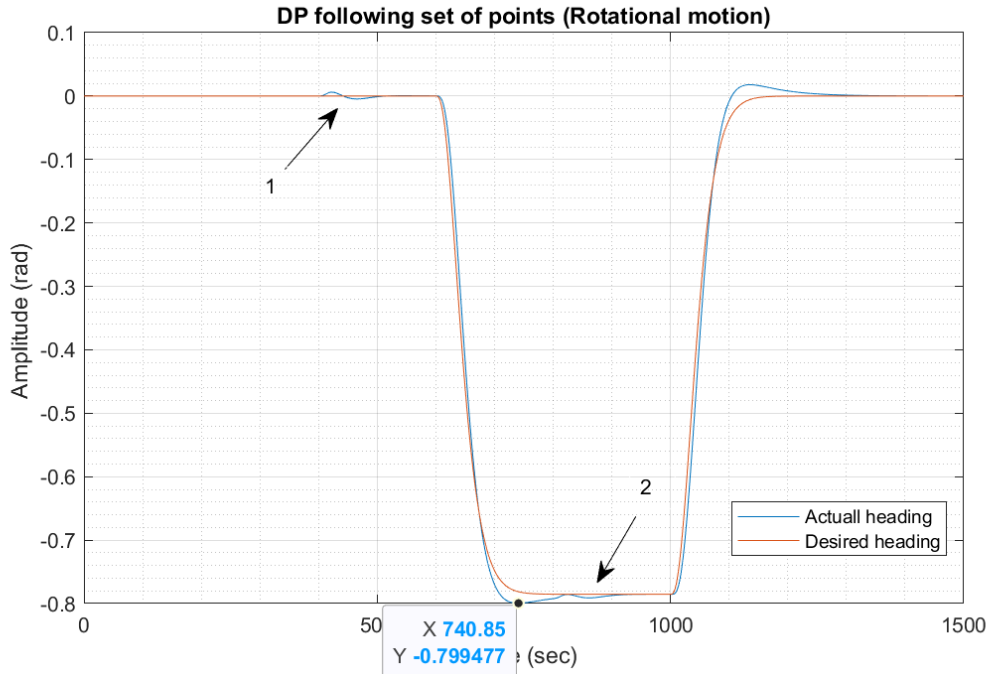


Figure 23: This figure represents the heading of the vehicle in the NED frame following a set of desired points without any environmental disturbances. The text boxes provide information about maximum overshoot happening in the system's heading, while the arrows are pointing at regions of interest to be discussed and explained.

In figure 23, it's noticed that the system is following the desired heading smoothly, but the overshoot can seem to be more than that in the position in 22. This behaviour is discussed before in 20a and can be enhanced by further tuning of the heading reference model. However, it's noted that disturbances similar to those in 22. there are 4 disturbances happening:

- **Disturbance 1 in figure 23:** It happens at time $t = 400\text{sec}$ when the vessel is:

- keeping position in North
- changing position in East
- is disturbed in heading

- **Disturbance 2 in figure 22:** It happens at time $t = 1000\text{sec}$ when the vessel is:

- changing position in East
- changing heading
- is disturbed in North

From this, we can deduct that the system can't keep all three states controlled (except for first 200 seconds as the system was already stable at the set point η_0). From this we can put a hypothesize a coupling in the dynamics of the vessel, which can be due to the following reasons:

- The ship is under actuated, hence, there are kinematic constraints to be fulfilled.
- The locations of the thrusters induce moments around the body frame of the vessel when moving in East direction. Moreover, the center of floatation (CF) is not the same as the body frame's origin (CB), hence, when the vessel tries to change heading, it rotates around the CF but the CB will be actually moved.

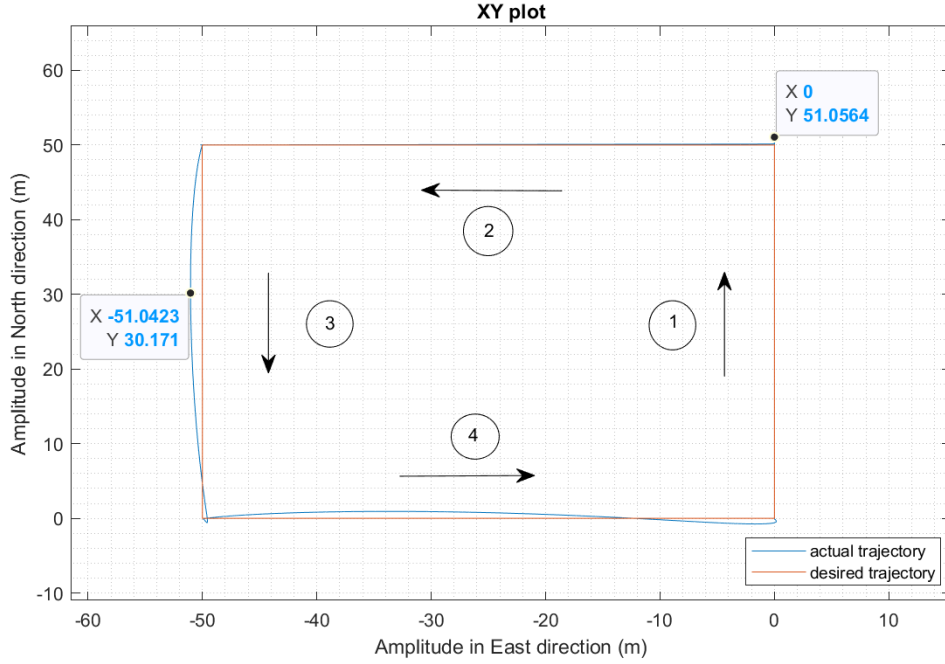


Figure 24: The following figure represents the xy-plot of the vehicle following the desired state. It shows arrows that represent the transition between states in NED frame. The boxes show maximum overshoot happening.

To discuss the performance of the system, the figure will be divided into 4 regions of interests (which are sides of the rectangle shown in 24 and annotated by arrows):

- **Transition 1:** pure translation in North direction. It shows perfect performance with minor overshoot at the end of the transition (1 meter)
- **Transition 2:** pure translation in West direction. Also with minor overshoot and very good performance.
- **Transition 3:** pure translation in South direction. However, the vessel is moving while keeping tilted heading (not 0 or 180). Thus, a deviation in X/East state of the vessel (Disturbance 1 in 22).
- **Transition 4:** pure translation in East direction. However, the vessel is moving while changing it's heading (from η_4 to η_5). Thus, a deviation in Y/North state of the vessel (Disturbance 2 in 22).

The previous discussion explains the behaviour of the vehicle. The following figure shows the xy-plot with vessel's heading annotated.

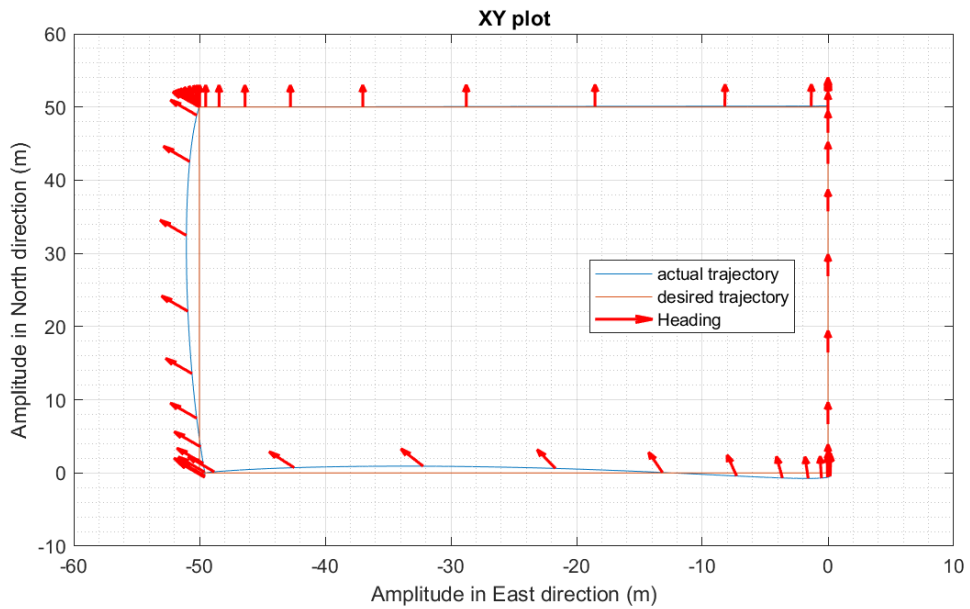


Figure 25: The following figure represents the xy-plot of the vehicle following the desired state. It shows arrows that represent the heading of the vessel, ψ

In 25, the arrows represent the heading of the vessel recorded every 1000 time-step. Hence, the sparsity of the arrows along a transition direction represents the rapid change of state, however, at the end of the transition, we see that the density grows and more arrows overlap. Thus, we can conclude that the system not only follows the trajectory in transient period, but also keeps it's state at the desired set point for some time before it chases after the next set point. This also shows that the allocated time 200sec was enough for the vessel to achieve it's goal.

11.2 Part 2

11.2.1 Simulation 1 - Environmental Loads

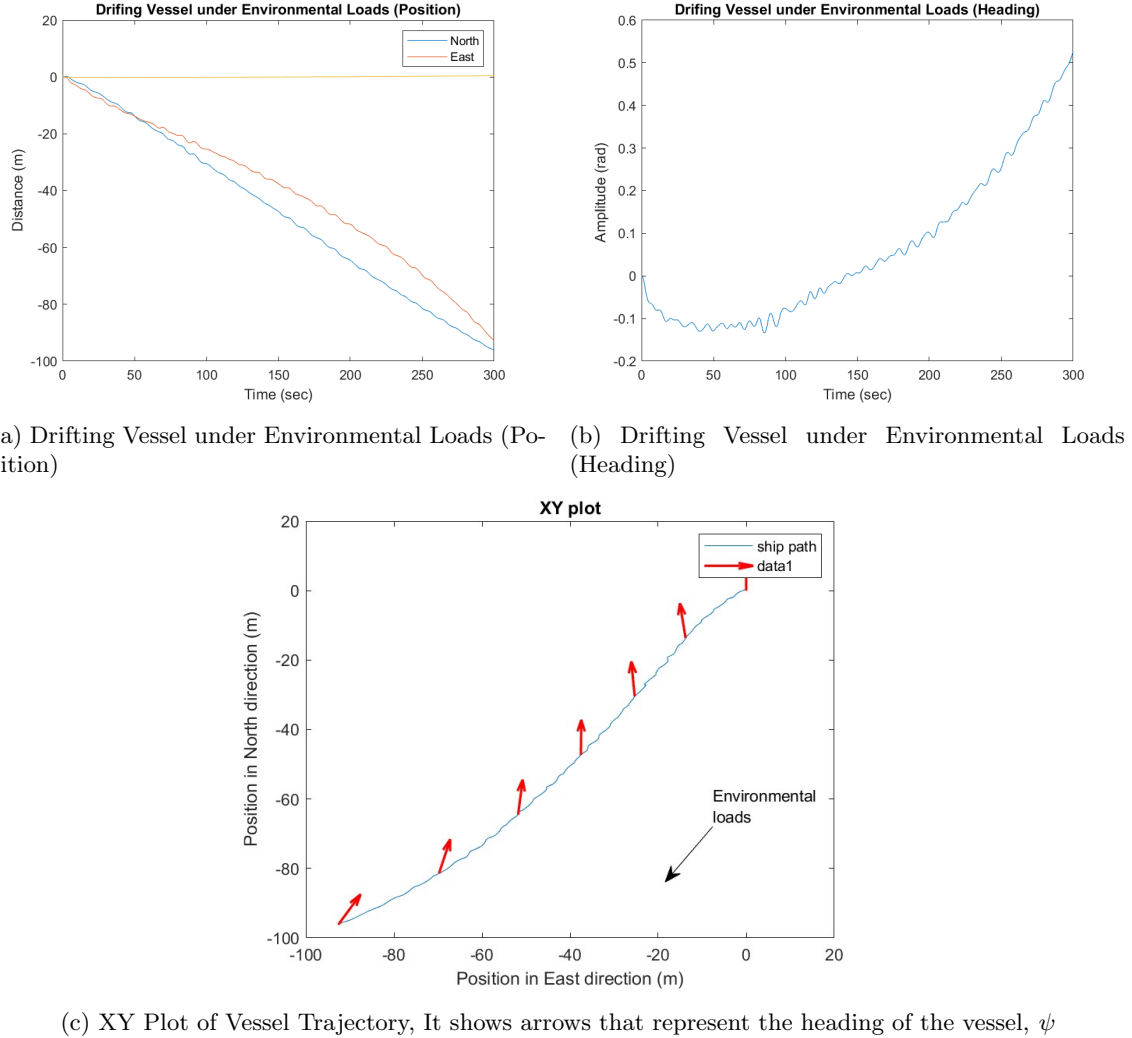


Figure 26: Plots demonstrating the vessel’s response to environmental loads inheading, position, and overall trajectory.

In Figures 26, in plot (a), the vessel’s Southwest drift is apparent, consistent with the directional influence of environmental loads. It is observed in plot (b) that there is a consistent variation in the vessel’s heading, measured in radians, suggesting a steady response to environmental forces. In figure (c) the XY plot demonstrates the vessel’s drift towards the Southwest, as indicated by the trajectory path with negative coordinates in both North and East directions. The red arrows signify the cumulative effect of wind, waves and current on the vessel’s movement. We observe that the vessel orient itself to minimize wind resistance when not under power.

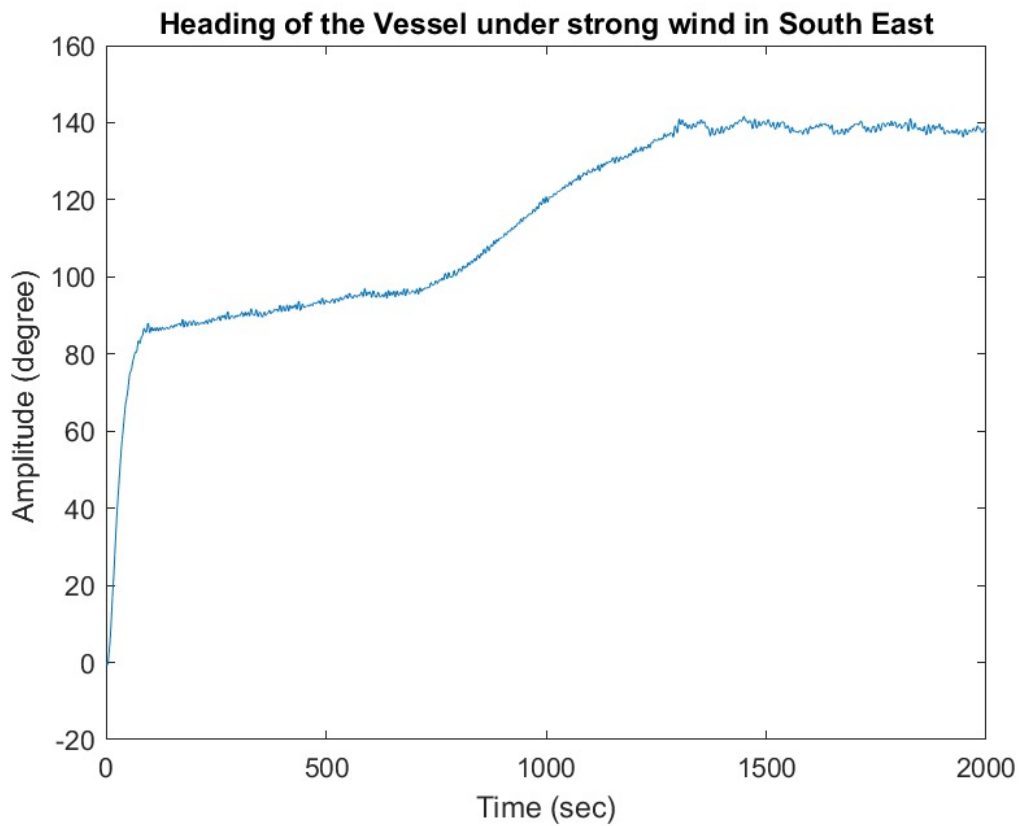


Figure 27: Drifting the vehicle under strong wind in south East

In Figure 27, we attempted to simulate the influence of a strong wind coming from the southeast at 135 degrees, while also increasing the simulation time. It was observed that the vehicle's heading consistently increased until it reached a heading of 135 degrees, after which the vehicle became stable.

11.2.2 Simulation 2 - DP and Thrust Allocation

Firstly, our result using quadratic programming

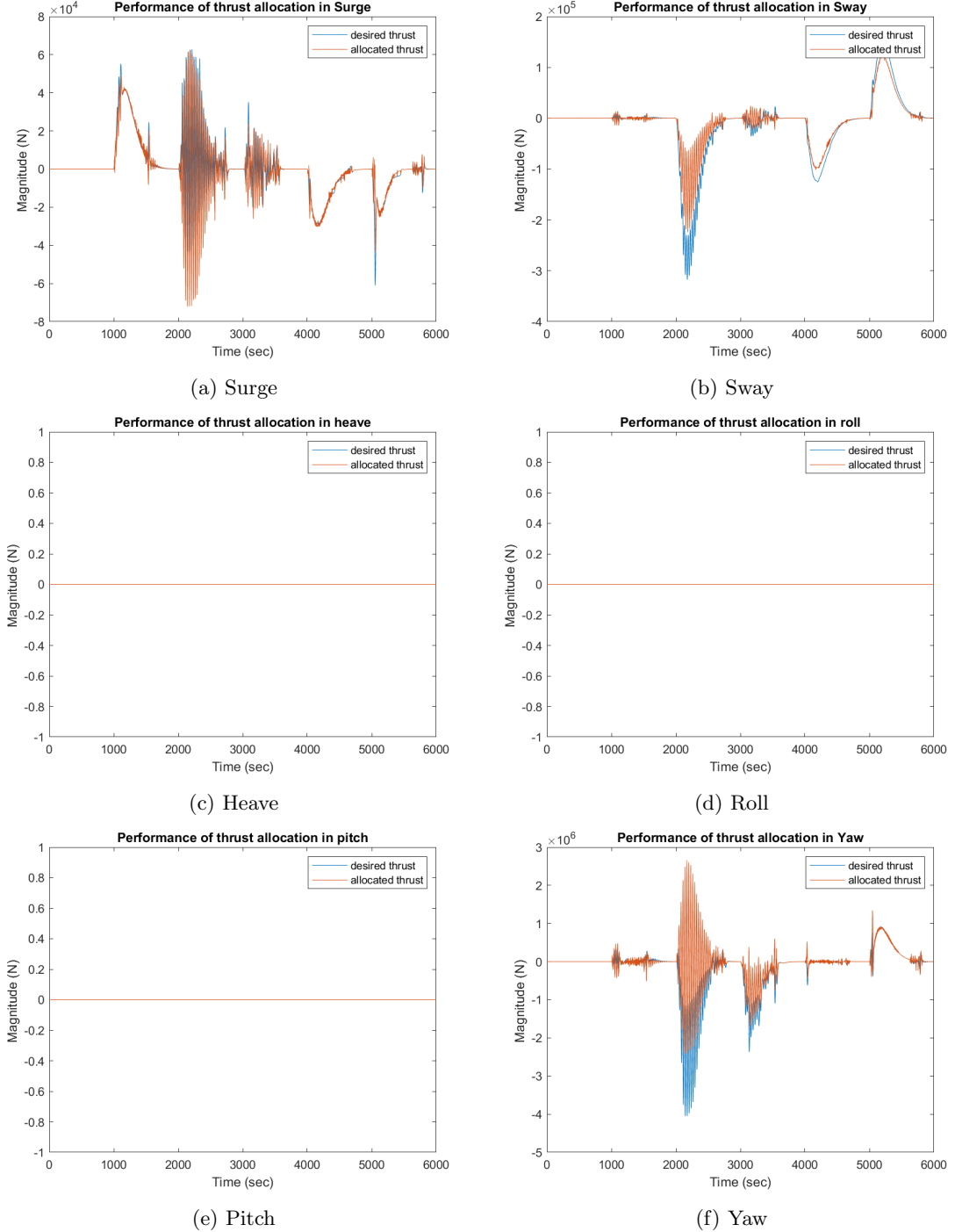


Figure 28: Performance of thrust allocation in various axes for quadratic programming .

In figure 28, it's observed that there is a discrepancy between desired and allocated thrust, notable in Surge, Sway, and Yaw. This indicates that our thrust allocation method, which utilizes quadratic programming, requires further tuning.

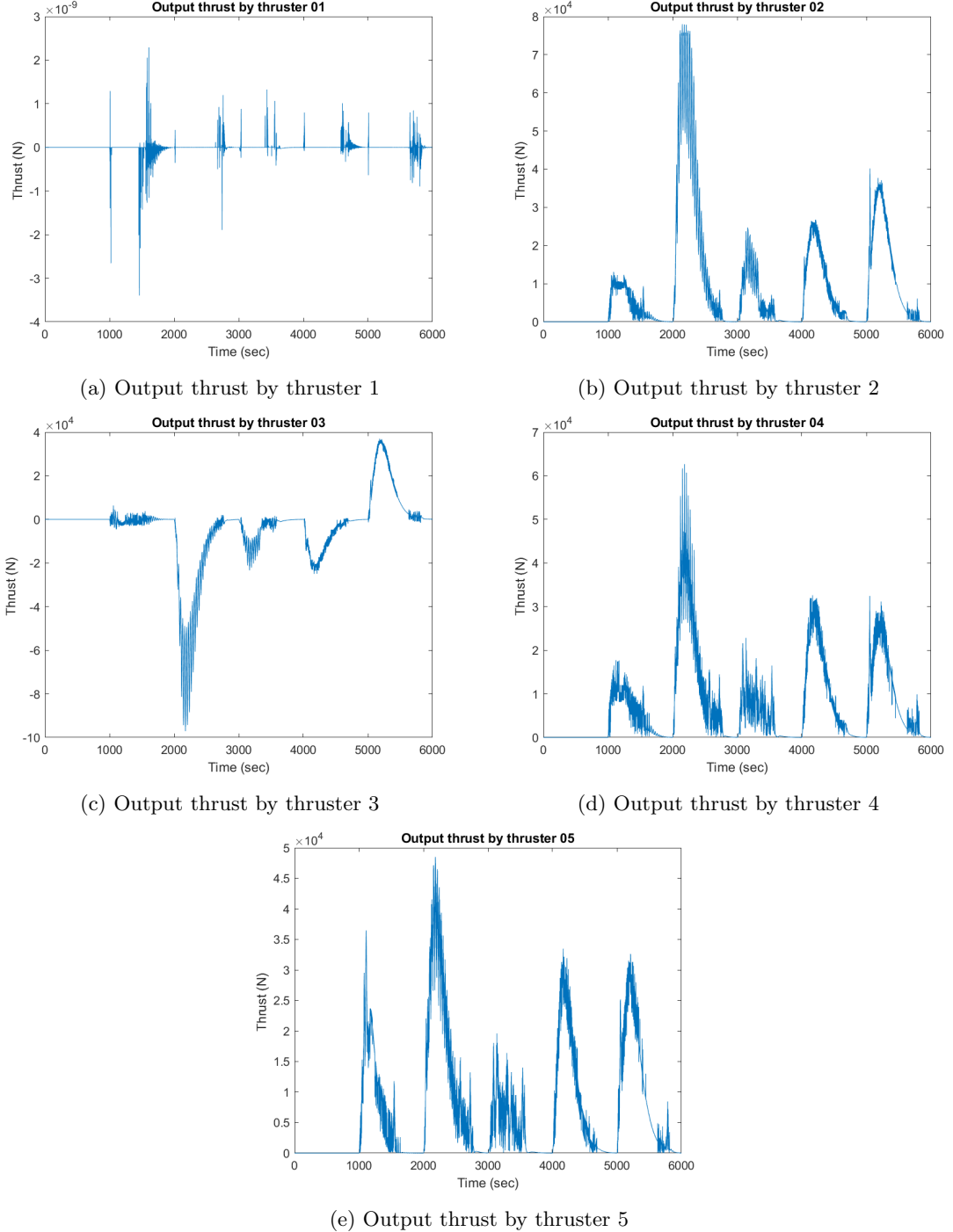


Figure 29: the output thrust u for all the thrusters for quadratic programming

In Figure 29, the thrust allocation using quadratic programming appears to be operational. However, the thrust output u for all thrusters exhibits significant fluctuations, suggesting instability and imprecise control. This indicates that further tuning of the quadratic programming is necessary.

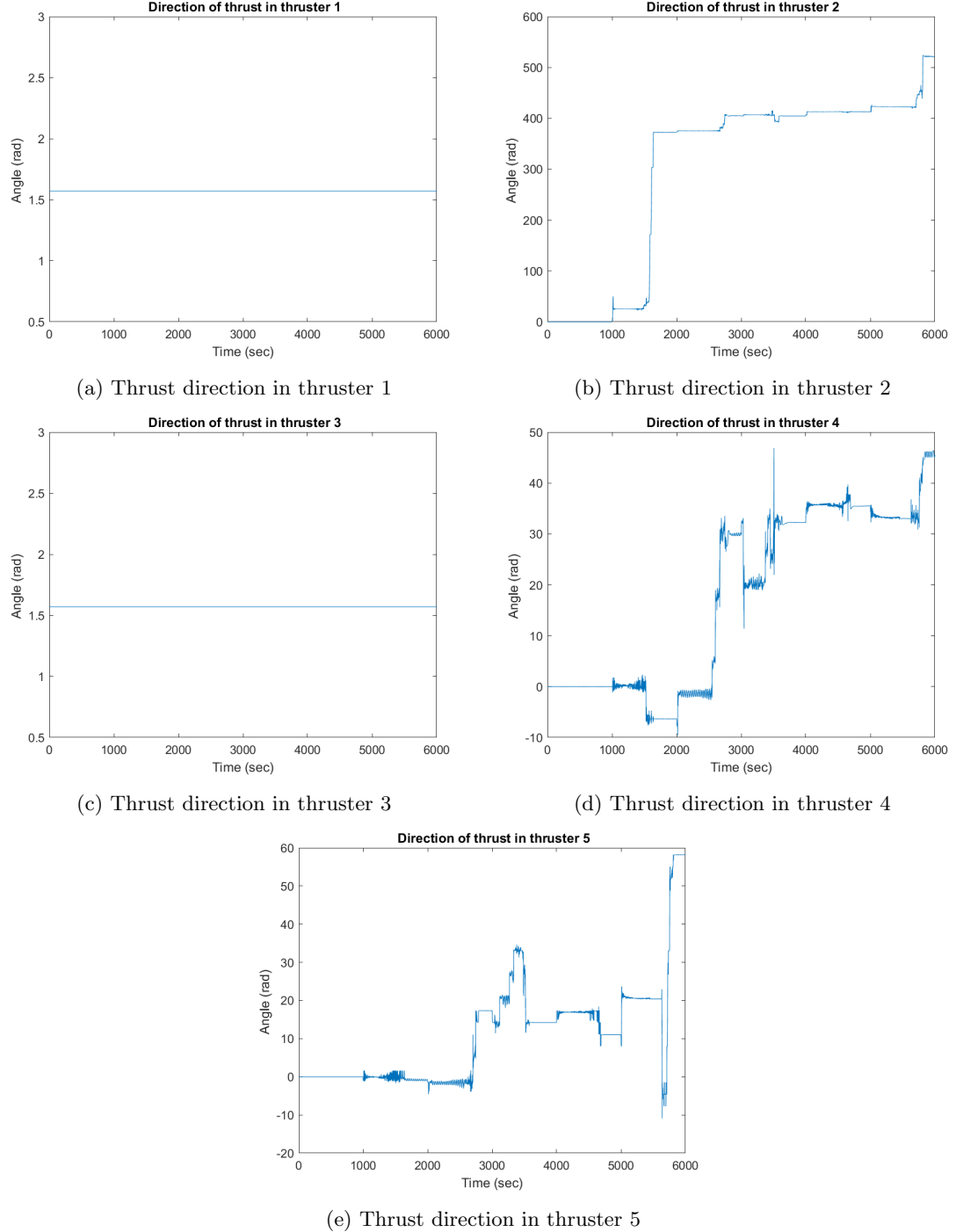


Figure 30: Observed thrust directions (Alpha) in various thrusters over time for quadratic programming .

In Figure 30, it is observed that thrusters 1 and 3 are fixed and maintain a constant angle, indicative of a 90-degree orientation, which corresponds to a radial angle of $\pi/2$ radians. The remaining thrusters are azimuth thrusters, showing significant fluctuation in their angles, which suggests instability in their control mechanisms and indicates the need for tuning to stabilize their response.

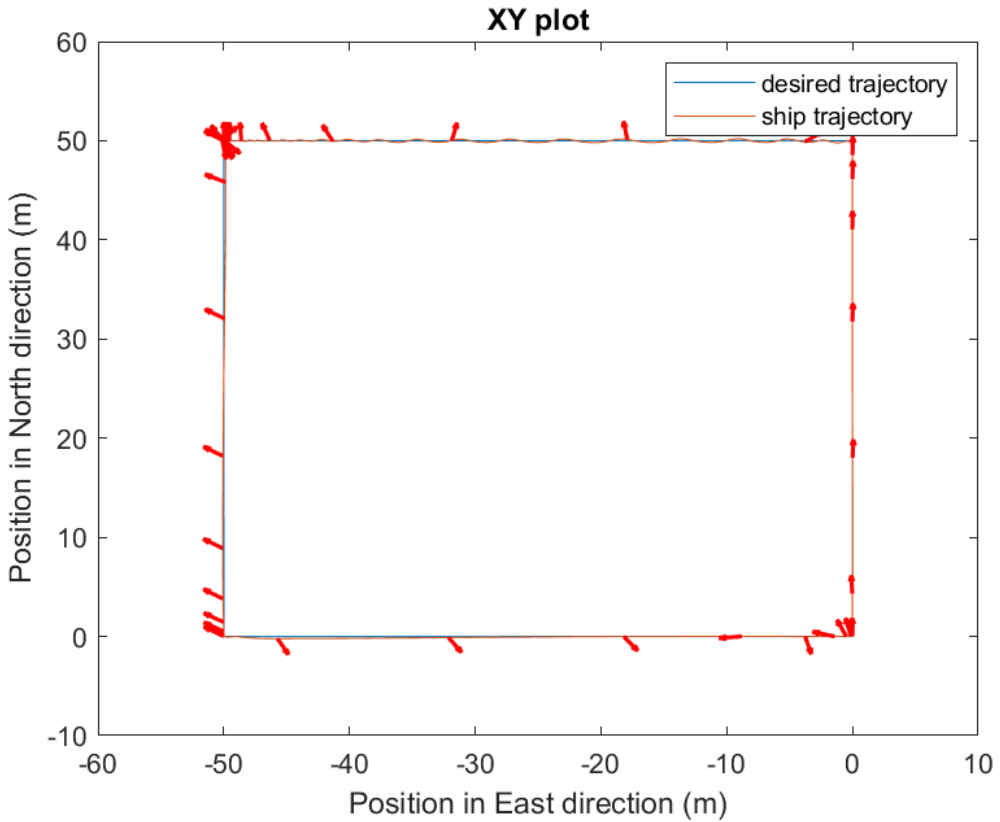


Figure 31: XY plot showing the ship's actual trajectory against the desired trajectory using quadratic programming.

In Figure 31, it is observed that the trajectories coincide well for the majority of the path, showing that the quadratic programming thrust allocation is working. However, fluctuations are observed at the turning points, particularly at the head, indicating potential overshooting. This behavior warrants investigation, especially since it occurs in the absence of environmental disturbances, which shows that our quadratic programming is not working well.

Secondly, We implemented the Pseudo inverse.

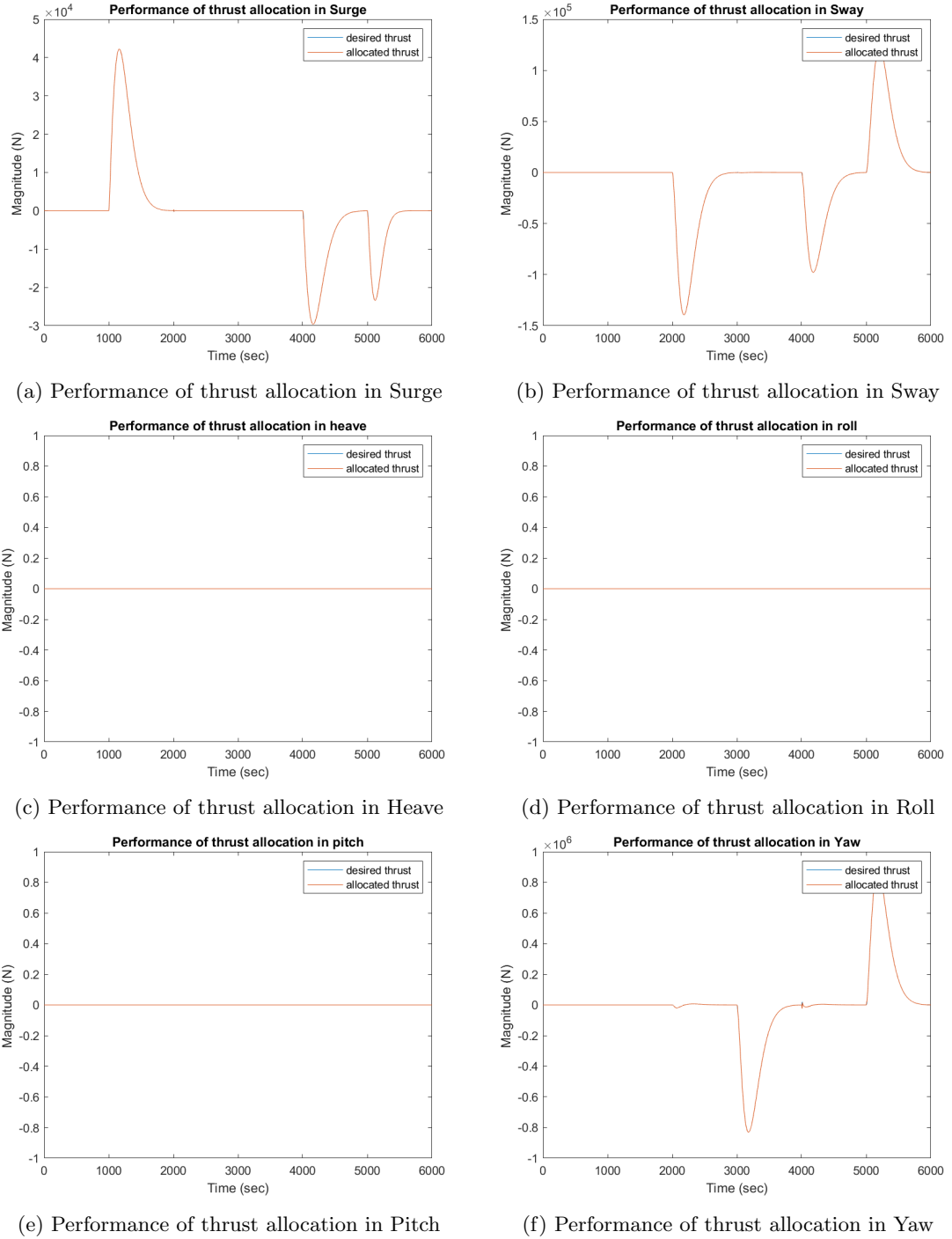


Figure 32: pseudo-inverse Performance of the thrust allocation in various Axeses

In figure 32, it is observed that the pseudo-inverse method for thrust allocation demonstrates a marked improvement over the quadrature programming method, with the allocated thrust more closely following the desired thrust profiles. Notable is the smoother response and reduced fluctuations, which indicate a more refined control and precision in thrust allocation. These results suggest that the pseudo-inverse method is more effective.

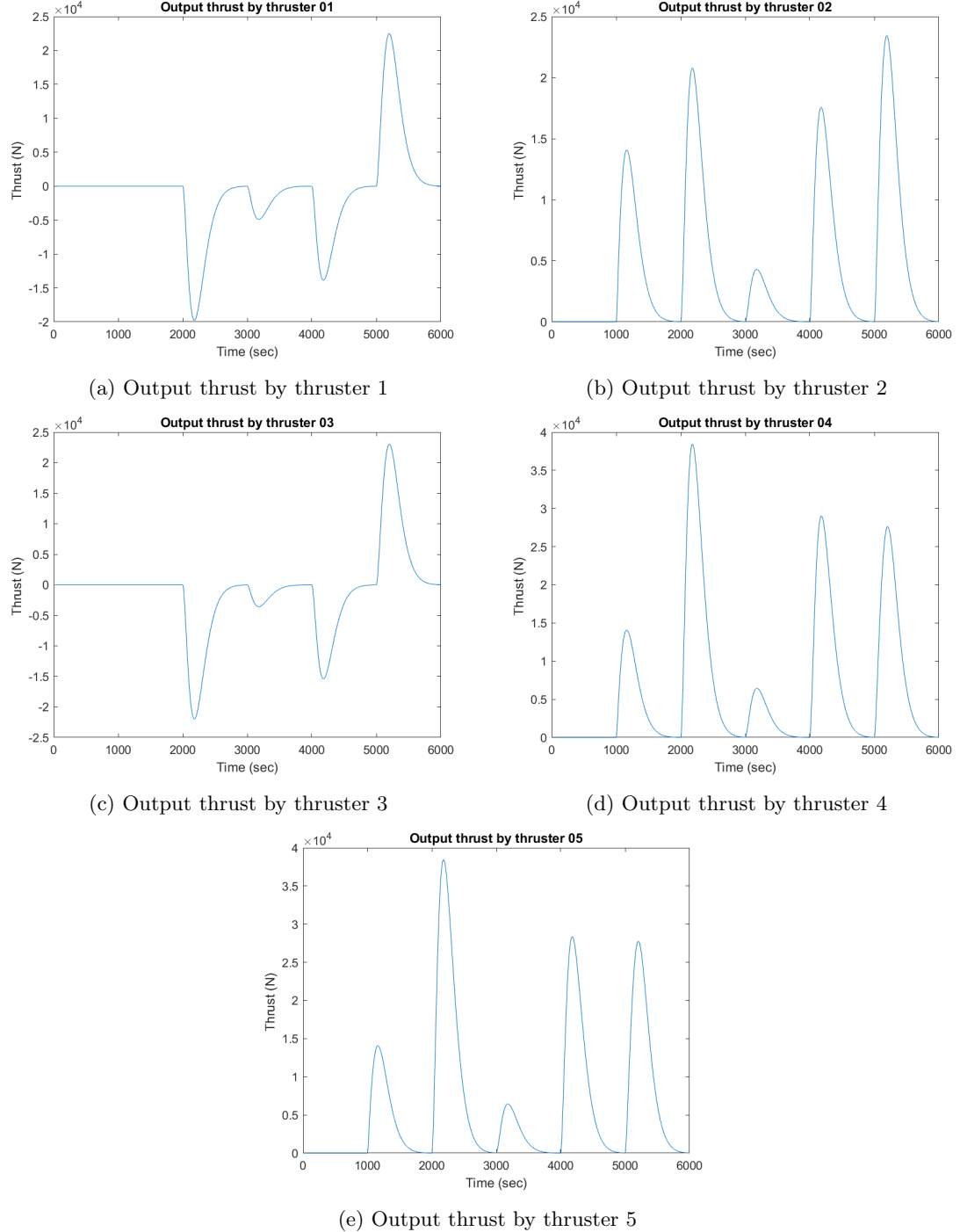


Figure 33: the output thrust u for all the thrusters for pseudo-inverse

In Figure 33, it is observed that using the pseudo-inverse method shows a consistent delivery of power without any fluctuations, while no thruster reaches the saturation as you see in all figures (because the controller does not ask for much effort output). Unlike the quadrature programming method, the pseudo-inverse approach results in a smoother thrust response without significant fluctuations, indicating a more robust and stable control.

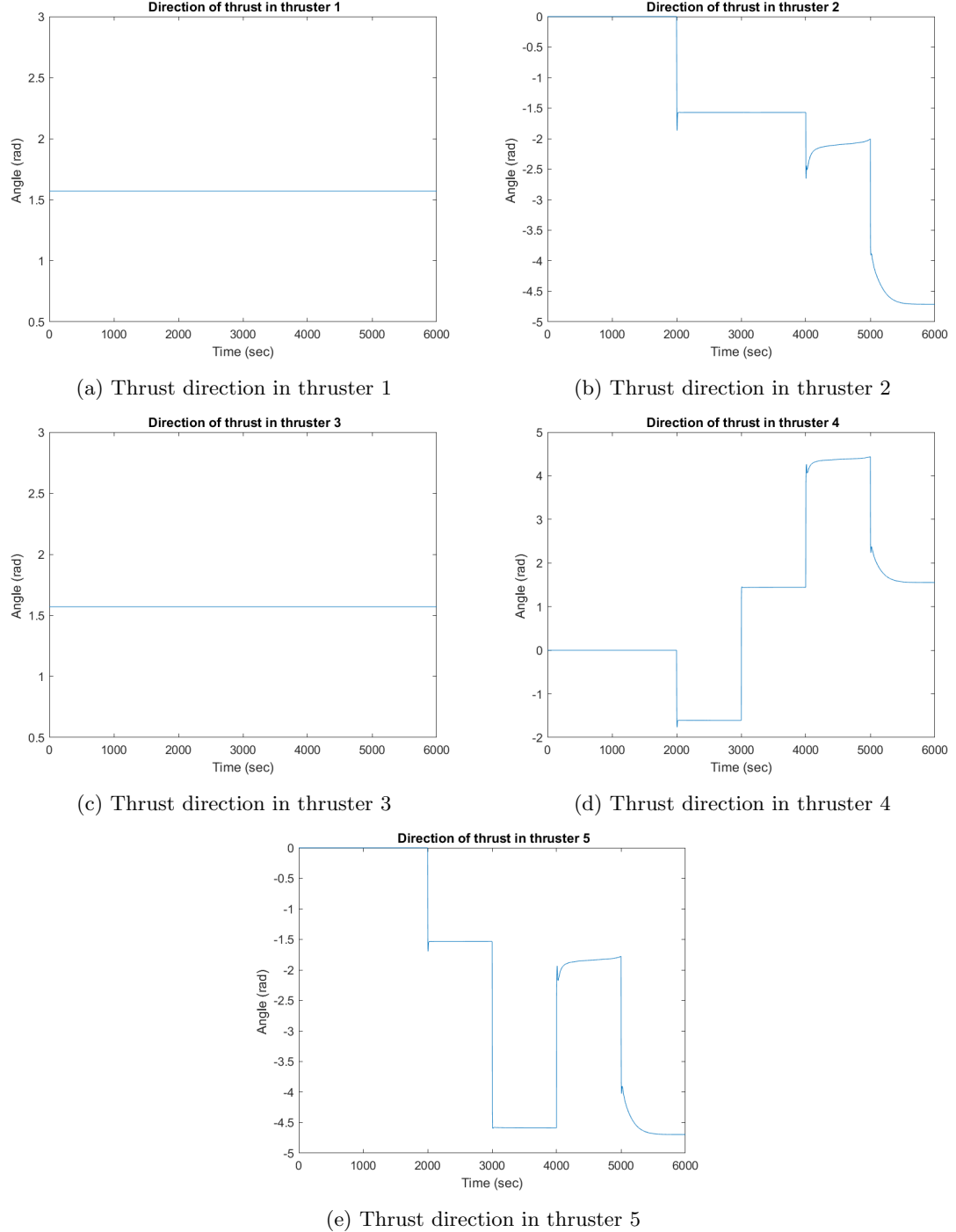


Figure 34: Observed thrust directions (Alpha) in various thrusters over time for Pseudo inverse.

In Figure 34, it's observed that the Pseudo inverse method is better than the Quadratic Programming. we can see that, thrusters 1 and 3 maintain a constant angle, indicative of a 90-degree orientation, which corresponds to a radial angle of $\pi/2$ radians. The azimuth thrusters are more stable compared to the fluctuations that we observed in the quadratic programming output.

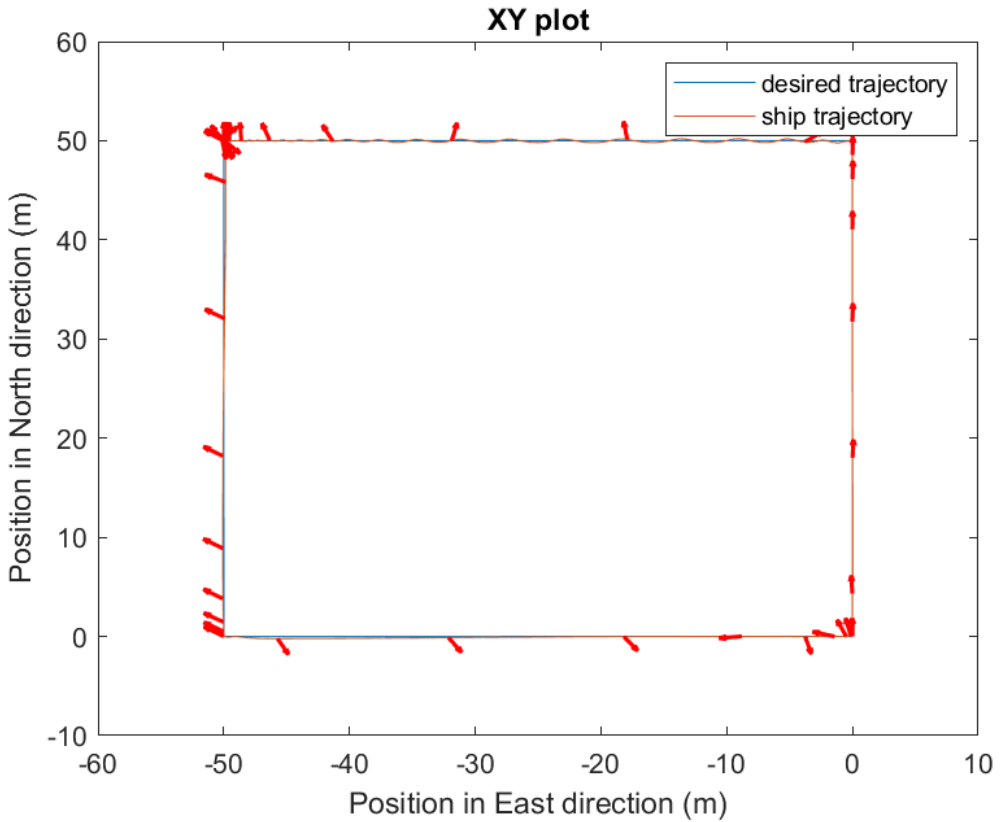


Figure 35: XY plot showing the ship's actual trajectory against the desired trajectory using pseudo inverse.

In Figure 35, it is observed that, in the absence of environmental disturbances, the desired trajectory coincides with the required trajectory in all cases. This demonstrates that our pseudo-inverse method is more effective than the quadratic programming approach.

when the thruster number 2 and 4 are disabled

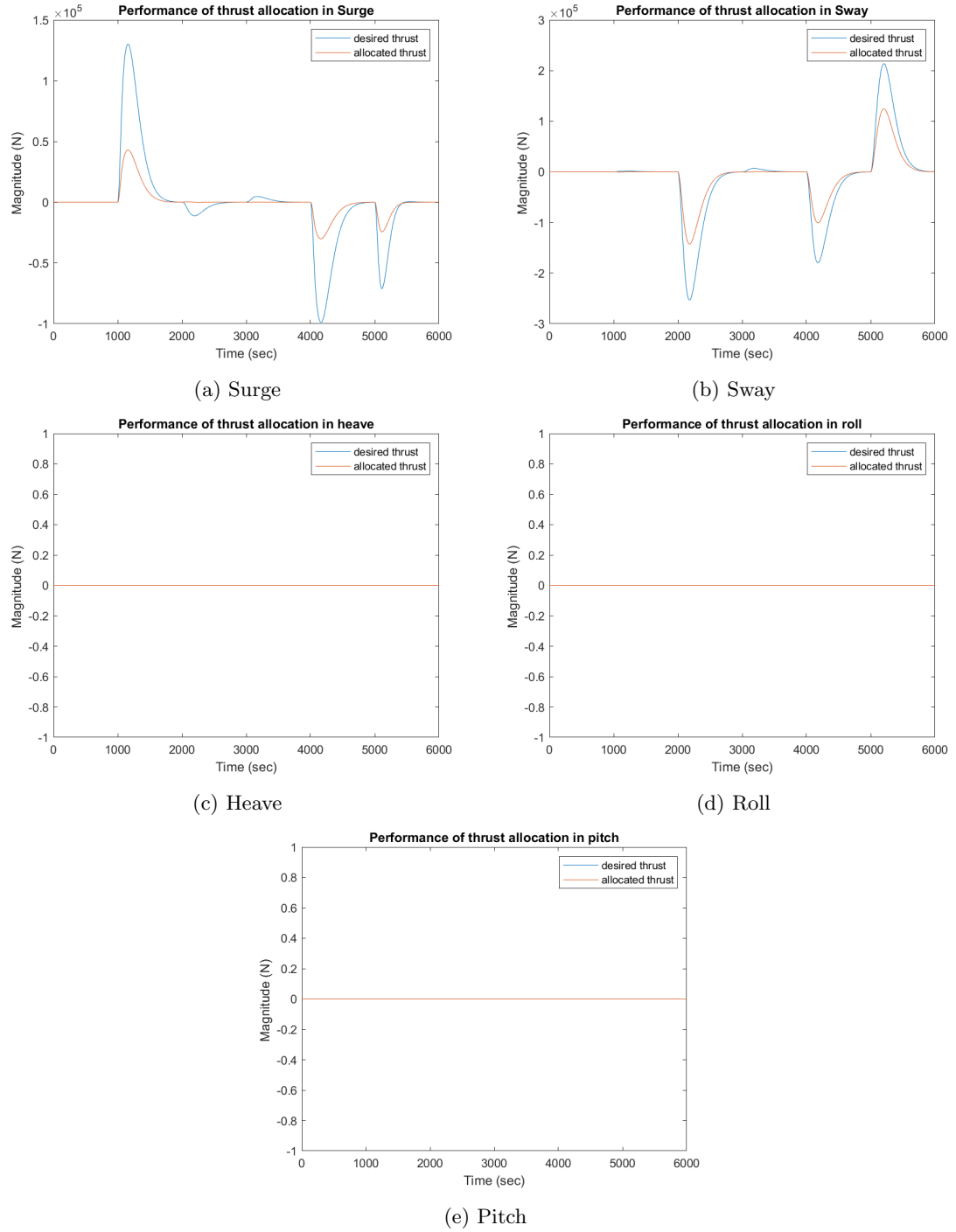


Figure 36: Performance of the thrust allocation in various Axeses when the thruster number 2 and 4 are disabled.

In Figure 36, it is observed that the impact on system performance when thrusters 2 and 4 are disabled, leading to a mismatch between the desired and the allocated as the given thrust not equal to the required thrust.

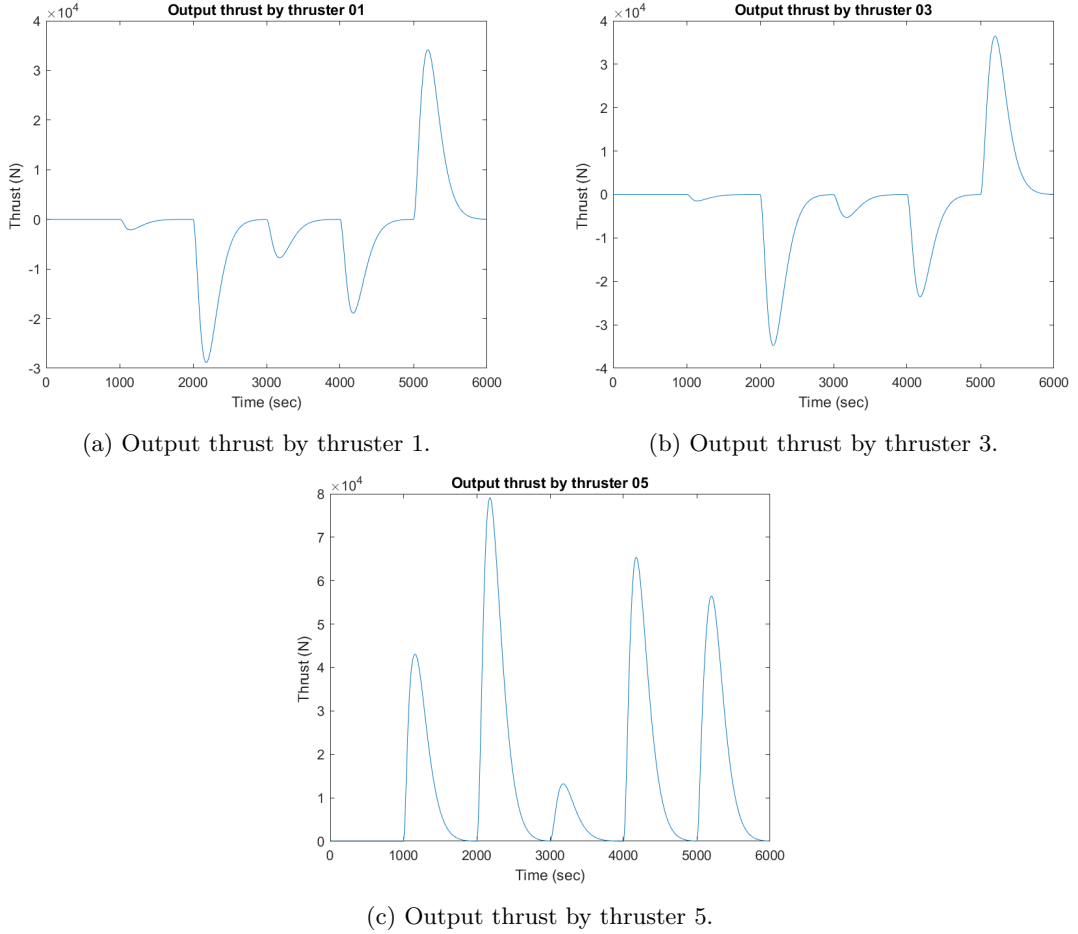


Figure 37: The output thrust u for thrusters 1, 3, and 5 when thrusters 2 and 4 are disabled.

Comparing Figures 37 and 33, it is observed that disabling thrusters 2 and 4 results in increased loads required from the thrusters for the vessel to be able to catch up with the reference model. It's then expected that output thrust for thrusters 1, 3, and 5 increase, as compared to the scenario where all thrusters are operational. This is demonstrated by maximum thrust in thruster 5 of (8×10^4), now compared to (4×10^4) in the previous simulation.

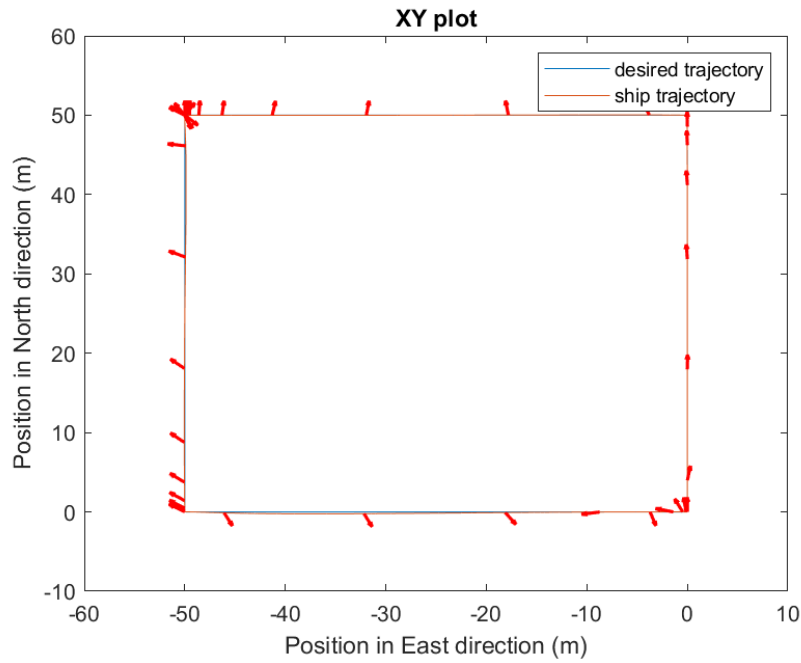


Figure 38: XY plot showing the ship's actual trajectory against the desired trajectory when the thruster numbers 2 and 4 are disabled.

In the figure, It's observed that even with some thrusters disabled, the vessel is still able to use the rest of the thrusters to follow the reference model. Which indicates that the thrust allocation model is working well demonstrated by a successful 4 corner test.

11.2.3 Simulation 3 - DP and Environmental Forces

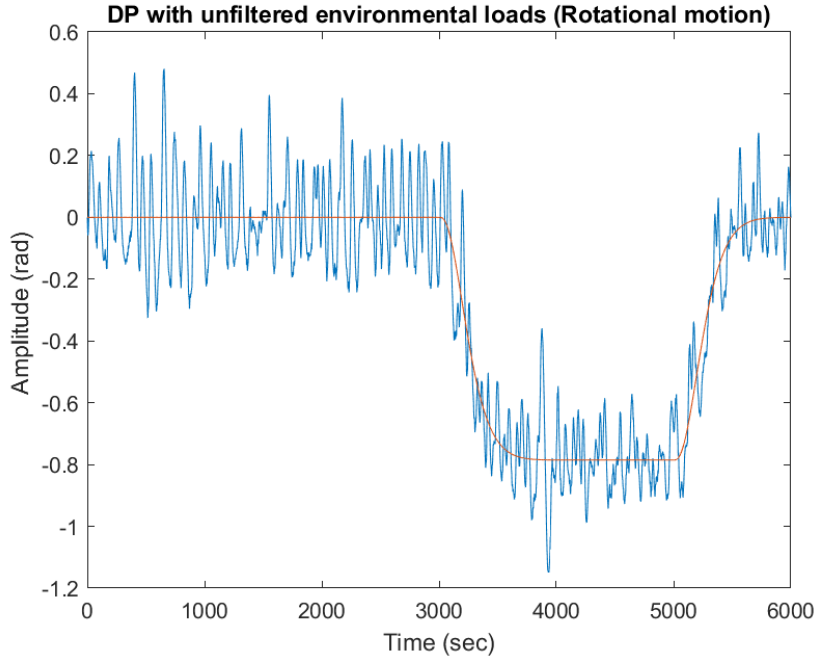


Figure 39: Rotational motion plot showing the actual trajectory in comparison to the desired trajectory.

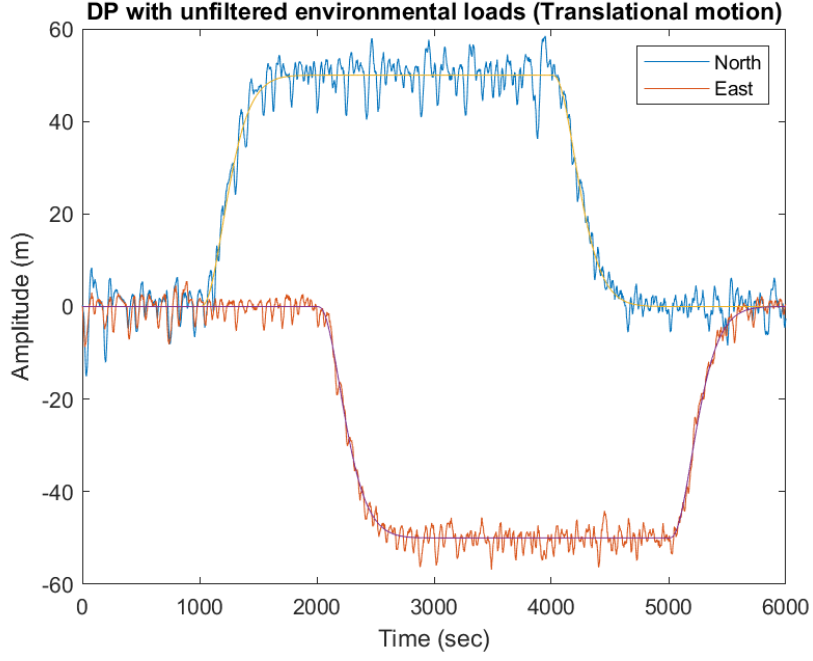


Figure 40: Translational motion plot for x and y.

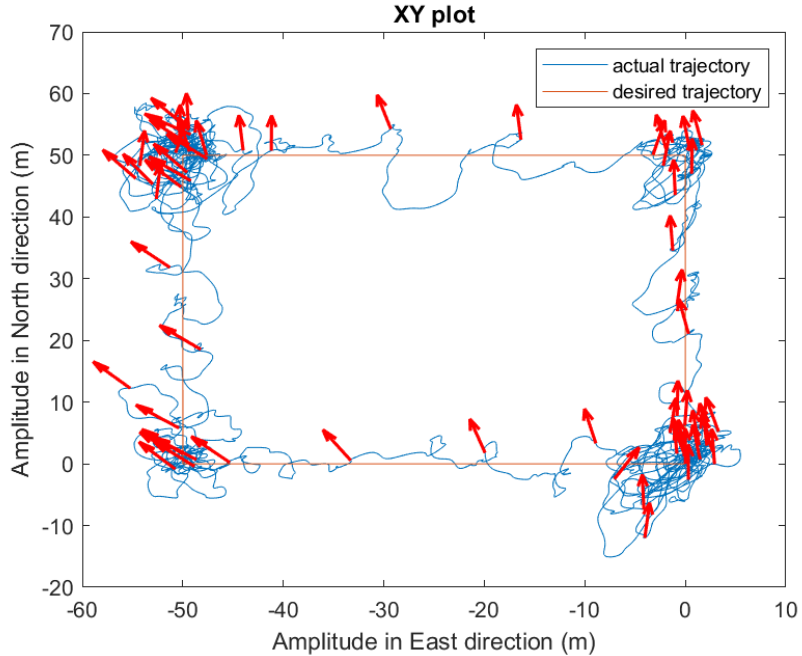


Figure 41: XY plot of the vessel's trajectory. The actual trajectory is marked in blue, and the desired trajectory in red, with arrows indicating the direction of movement.

In Figures 39 and 40, it is observed that the high frequency of the waves causes fluctuations in the actual trajectory, revealing discrepancies caused by the absence of an observer in the control system, what means that all the high frequency signal is passed to the controller, which will, in return, request for high frequency thrust. This absence is evident in the system's inability to dampen these fluctuations.

In Figure 38, it is observed that the control system, lacking an observer, struggles to handle

high-frequency waves, resulting in the actual path deviating significantly from the desired path.

11.2.4 Simulation 4 - Observer selection

In this simulation, we used the same environmental conditions as in Simulation 1. The desired Dynamic Positioning (DP) force was fixed at $\mathbf{DP} = [1 \ 1 \ 1] \times 10^4$. The simulation time was set to 300sec. We compare the observer output with the real measurements (with and without wave forces/moment)

With wave forces/moment

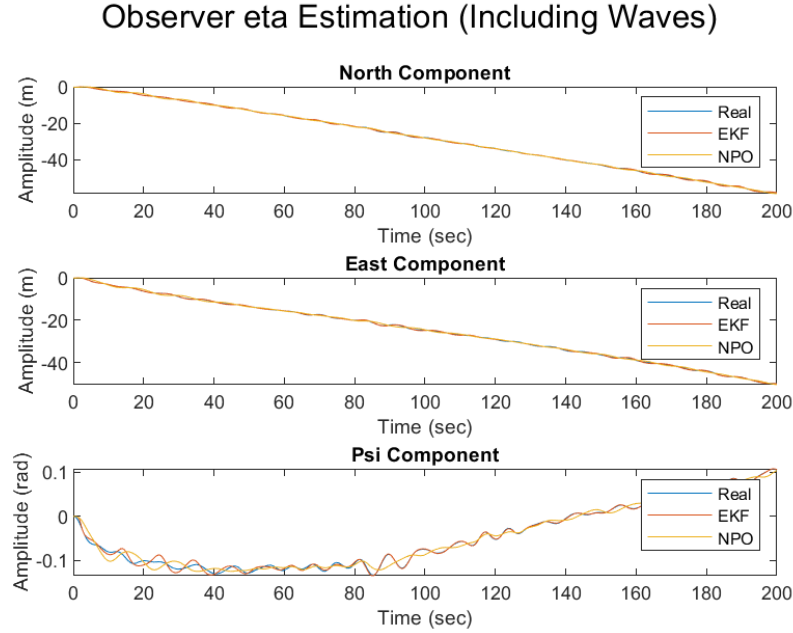


Figure 42: Comparison of the North, East, and Psi components of the observer output with the real measurements under full environmental forces. The Extended Kalman Filter (EKF) and Nonlinear Passive Observer (NPO) are plotted against the true values (Real) showing the tracking performance over time.

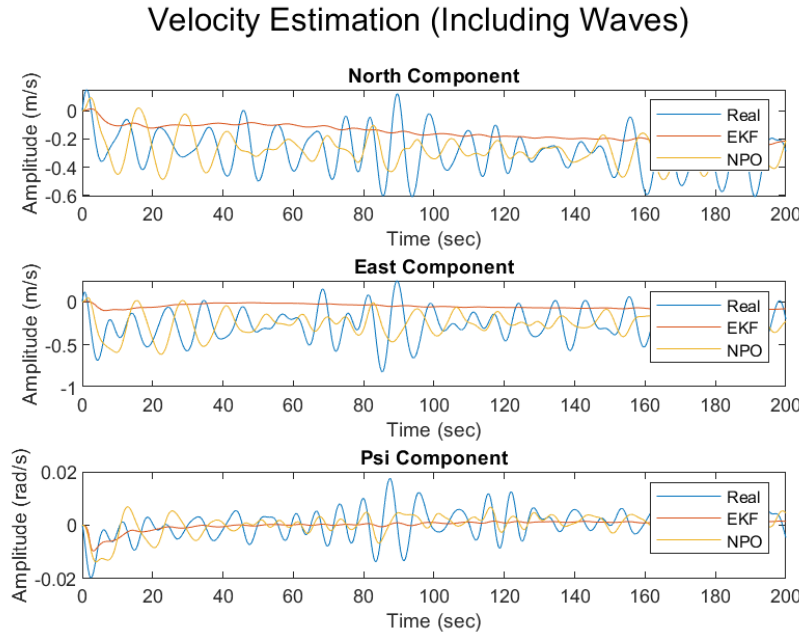


Figure 43: Velocity estimation graphs for North, East, and Psi components, including the influence of wave forces. Both the EKF and NPO observers are compared against the real measurements, illustrating the effect of environmental disturbances on velocity estimation.

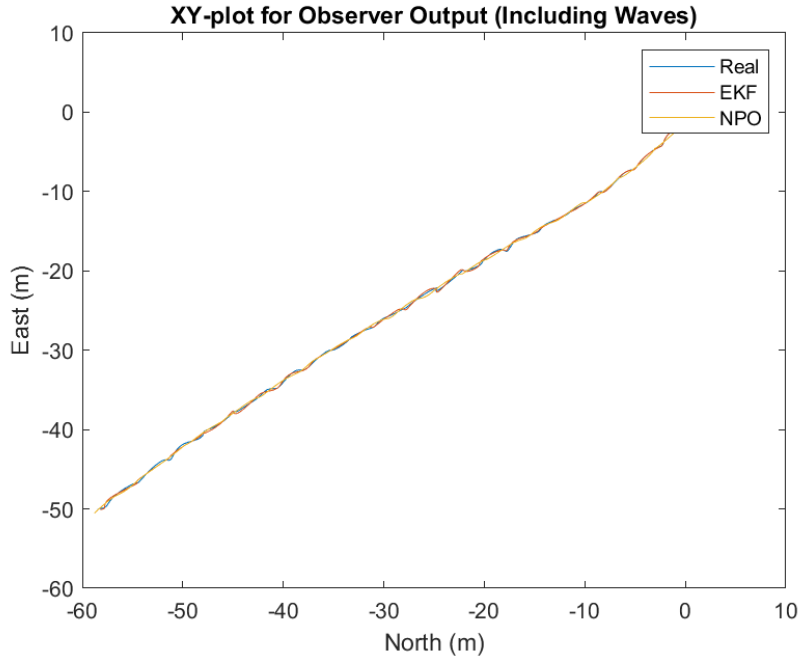


Figure 44: XY-plot of observer outputs for path tracking with wave forces included. The plot demonstrates the path tracking accuracy of the EKF and NPO observers compared to the real trajectory.

In this simulation, EKF and NPO shows good tracking accuracy for the north and east components, while EKF has more oscillation in psi estimation. However, EKF shows smoother output in the velocity estimation compared to NPO.

Without wave forces/moment

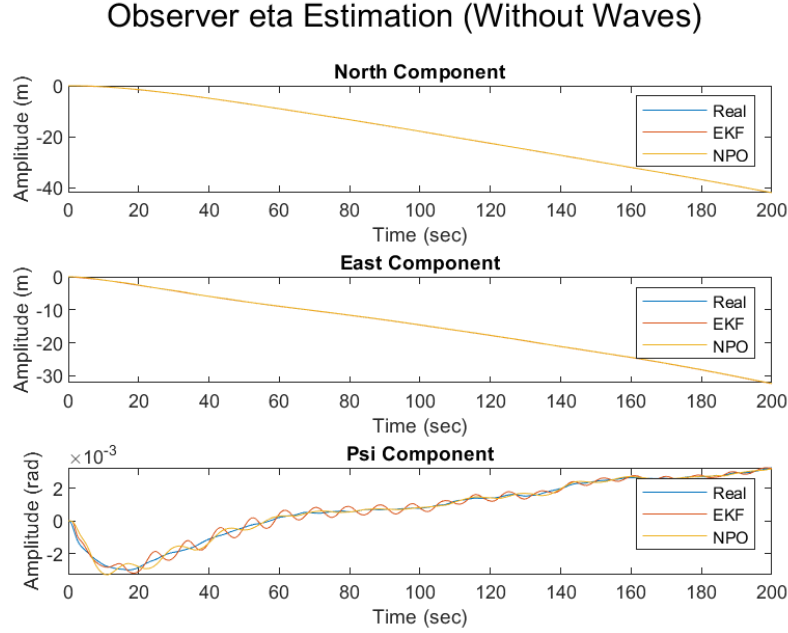


Figure 45: Comparison of the North, East, and Psi components of the observer output with the real measurements without considering waves forces/moment. The Extended Kalman Filter (EKF) and Nonlinear Passive Observer (NPO) are plotted against the true values (Real) showing the tracking performance over time.

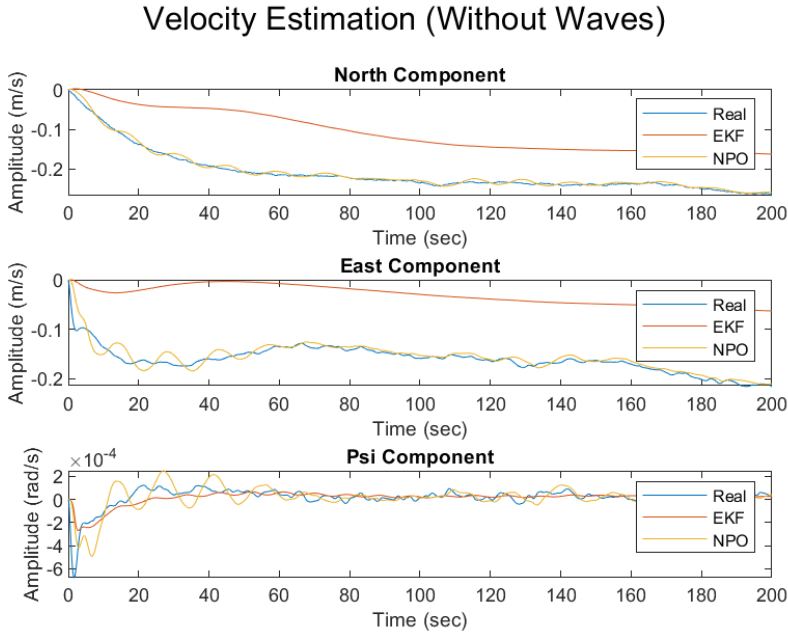


Figure 46: Velocity estimation graphs for North, East, and Psi components, without the influence of wave forces. Both the EKF and NPO observers are compared against the real measurements.

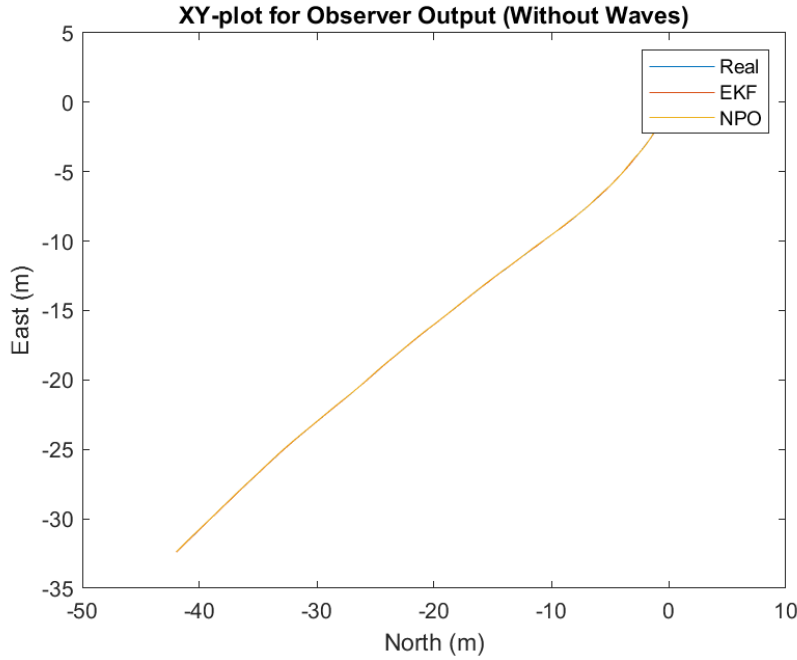


Figure 47: XY-plot of observer outputs for path tracking without wave forces/moment. The plot demonstrates the path tracking accuracy of the EKF and NPO observers compared to the real trajectory.

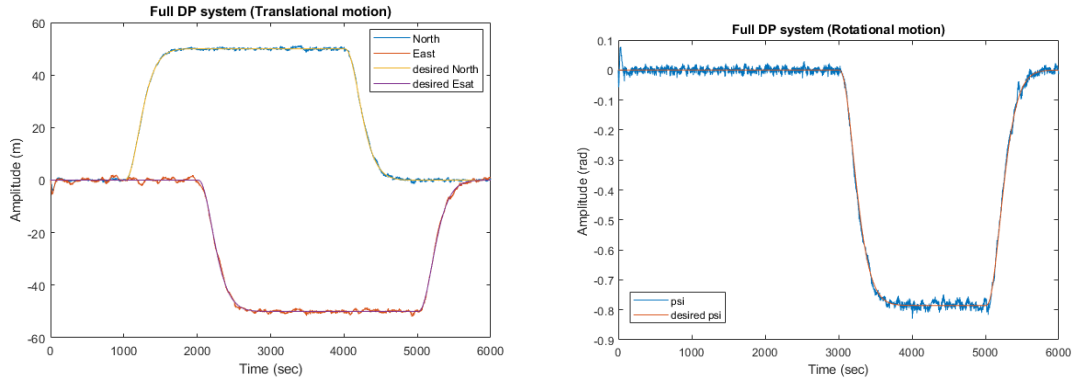
In this simulation, EKF shows more oscillation in psi estimation. Also, It has smoother output in the velocity estimation but it has an offset. NPO exhibits high oscillation in velocity estimation.

Observer selection

EKF and NPO shows acceptable tracking accuracy for eta estimation in both cases (with and without waves forces/moment) according to figures (42, 45). Moreover, EKF shows greater performance in velocity estimation compared NPO. NPO shows higher fluctuation in velocity estimate over time. This behaviour will affect the controller as velocity estimate tracks the real measurements. This means that the noises and the wave effect wasn't completely filtered by NPO according to figures(43, 46). We will choose EKF as it gives better estimation for state of the vessel (η, ν) in both cases (with and without waves) and show better performance for wave filtering and reduce the process and measurement noises. However, the output of our EKF can be improved by further tuning the filter parameters to dampen the oscillations in psi estimation and remove the offset in velocity estimation.

11.2.5 Simulation 5 - Complete Simulation

In this simulation, according to previous tests, we are going to carry out a simulation, utilizing all parts of the DP system, for tracking a sequence of states which are mentioned in part 1. We are using pseudo inverse as a thrust allocation algorithm and the EKF as our observer, with PID controller and a reference model system to have smoother trajectories.



(a) vessel's position in North and south directions w.r.t desired positions
(b) vessel's position in North and south directions w.r.t the desired Heading

Figure 48: Full DP system performance in the 4 corner test under full environmental loads, current, wind, and waves, using EKF as an observer. The figures shows vessel's state η (North, East , Psi) w.r.t desired state

In Figures (48a , 48b), the system follows the desired trajectory with some oscillations due to the high frequency waves. Compared to figures (40 , 39) the system is following the reference model in far more stable way. This shows that our observer succeeded in filtering out high frequencies form the vessel's state, even though the EKF needed further tuning. Figure 48a shows better response in tracking the desired north trajectory than in tracking the desired east, which is clear from the low frequency oscillation of the vessel around the zero line in the first 2000 second. This issue can be addressed by further tuning of the PID controller in the East direction, because the performance of the EKF in predicting the east component is acceptable as shown in Figure 42. It's also clear that the oscillations around the desired set-points is much less during transitions, i.e. from 0 to 50 in north direction, than those when trying to keep the vessel in a state , i.e. 50 in north. This is because the transition time is shorter, as implemented in our reference model.

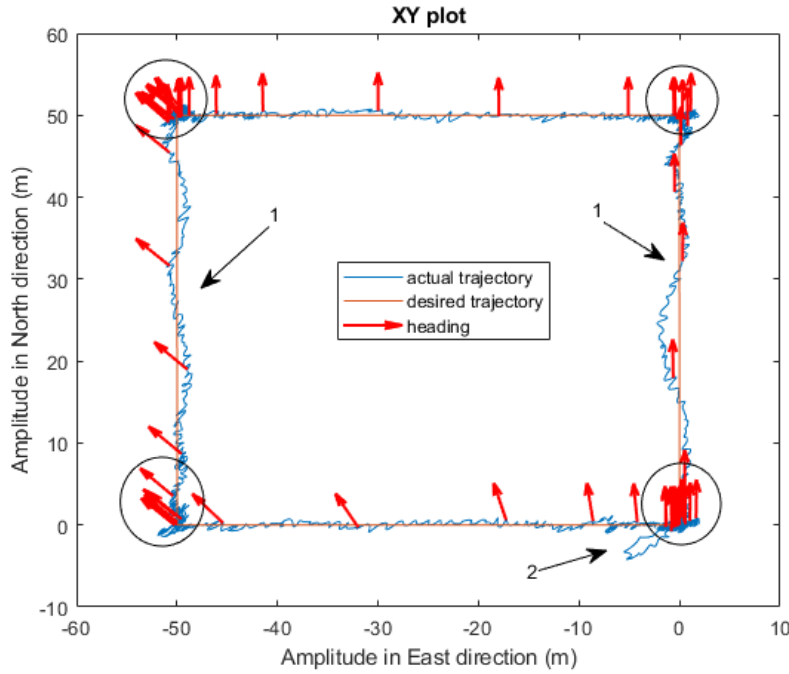


Figure 49: XY plot showing the vessel's performance in the 4 corner test. The vessel's position is represented by blue curves while the heading is represented by red arrows. The desired path is plotted as orange-colored square. Arrows and circle's are pointing to areas of interest which are to be discussed.

In Figure 49, the oscillations in east component's control is very clear as indicated by arrows (no.1). On the other hand, the north component control's performance is much better. In spite of the oscillations induced by the environmental conditions, it's clear (from the circles at the corners) that the vessel is also following the heading trajectory very well. The high concentration of the arrows at the corners indicates that the vessel is keeping its desired state for some time, which shows the system's capability to fullfil the desired state, even with suboptimal tuning parameters of the PID and the EKF, which can be enhanced more.

11.2.6 Simulation 6 - Capability Plot

We have used the simulation parameters, which are

- Simulation time = 200 sec
- Observer = EKF
- Thrust allocation = Pseudo inverse allocation method
- Full enviromental forces (current, wind and waves)
- Fixed weather condition, $U_c = 0.2 \text{ m/s}$, $H_s = 4.0 \text{ m}$ and $T_p = 8.0 \text{ s}$, $U_3 = 12.0 \text{ m/s}$.
- Fixed set point $\eta_{sp} = [0, 0, 0]$

We have changed the environmental direction with increment of 10 degrees in range (0 – 360) for current, wind and waves. We have computed the average thrust percentage against the environmental direction for wind, current and waves and made two capability plots in two cases

Without constraints

Figure 50 shows that the average thrust percentage is much higher in third and fourth quadrants compared to the first and second quadrants. This means the environmental forces on the vessel has high impact in the third and forth quadrants. Overall, the average thrust utilization doesn't exceed 60 percent to keep the vessel at the set point.

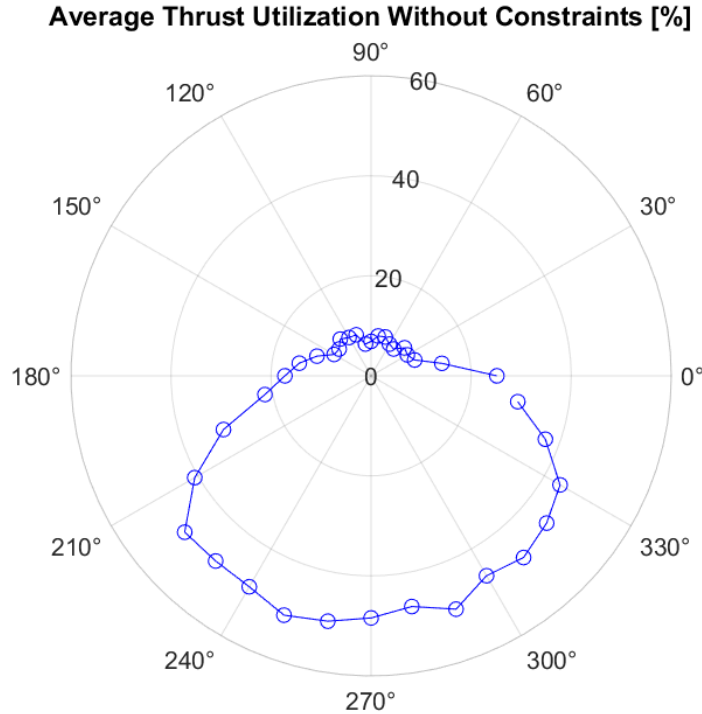


Figure 50: Average Thrust Utilization Without Constraint

With constraints

We set the following constraints

- Position deviation to be less or equal 3 m
- heading deviation to be less or equal 3 degrees

Figure 51 shows that DP system doesn't succeed to keep the vessel at the set point given these environmental forces. This means that the we need to further tune the observer and the PID controller. One possible reason for the constraint violation at these cases is that DP system is not fast enough to react to the environmental forces. This means the vessel deviates so much at the beginning of the simulation, then the DP manages to bring it back to the set point

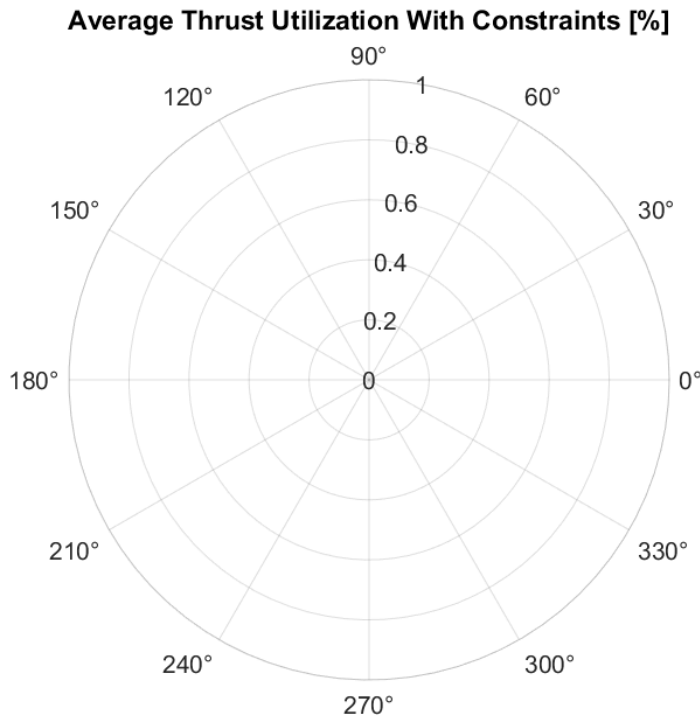


Figure 51: Average Thrust Utilization With Constraint

11.2.7 Simulation 7 - Observer robustness

By changing the wave height to 8 [m] and period to 13[s], then plotting the vessel position 2000 seconds, for station keeping at the origin ($\eta_{SP} = [0 \ 0 \ 0]$), we can see if the observer is still helping with the station keeping. In order to evaluate if the selected observer is robust or not, the simulation is carried out in three cases:

- With no observer
- With the NPO as an observer
- With the EKF as an observer

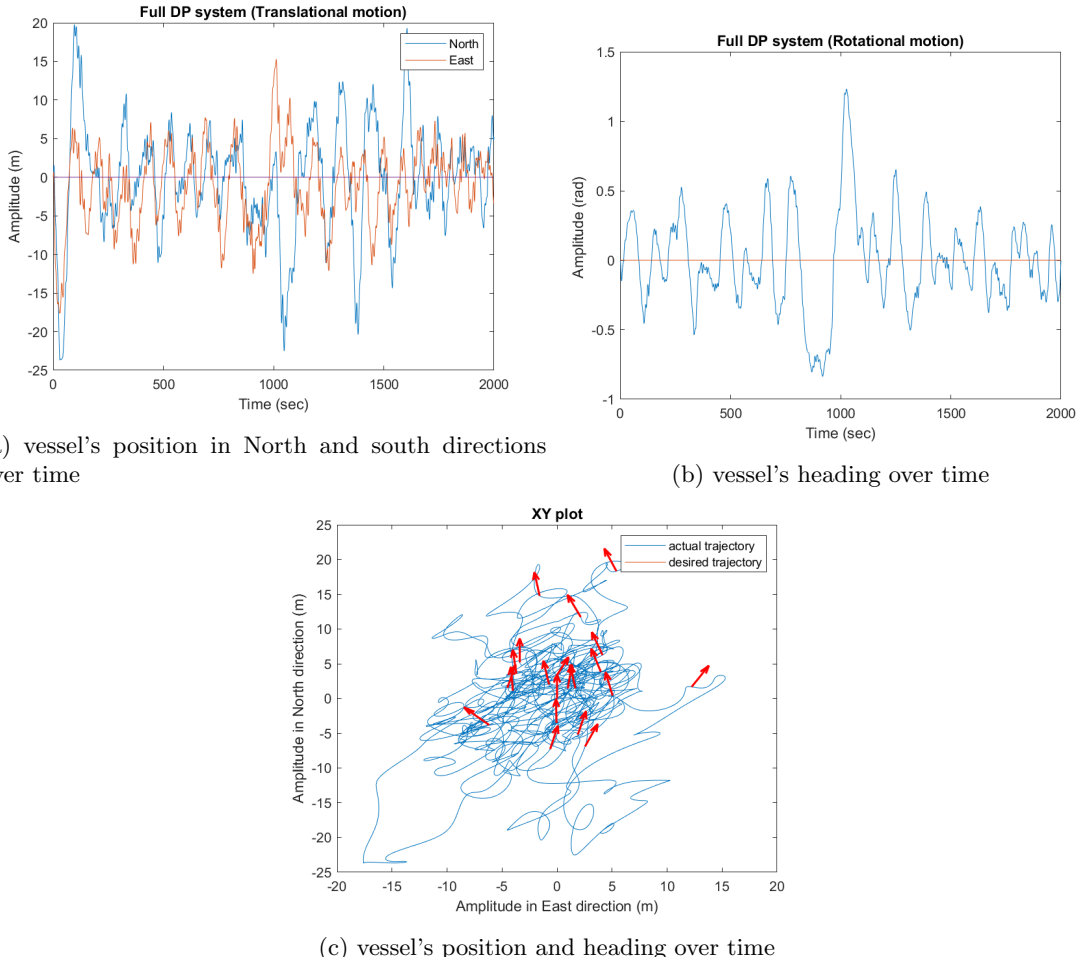


Figure 52: Full DP system performance in station keeping at $\eta = [000]$ test under full environmental loads, current, wind, and harsher waves, without observer. The figures shows vessel's position η (North, East) as blue curve and heading, represented by red arrows

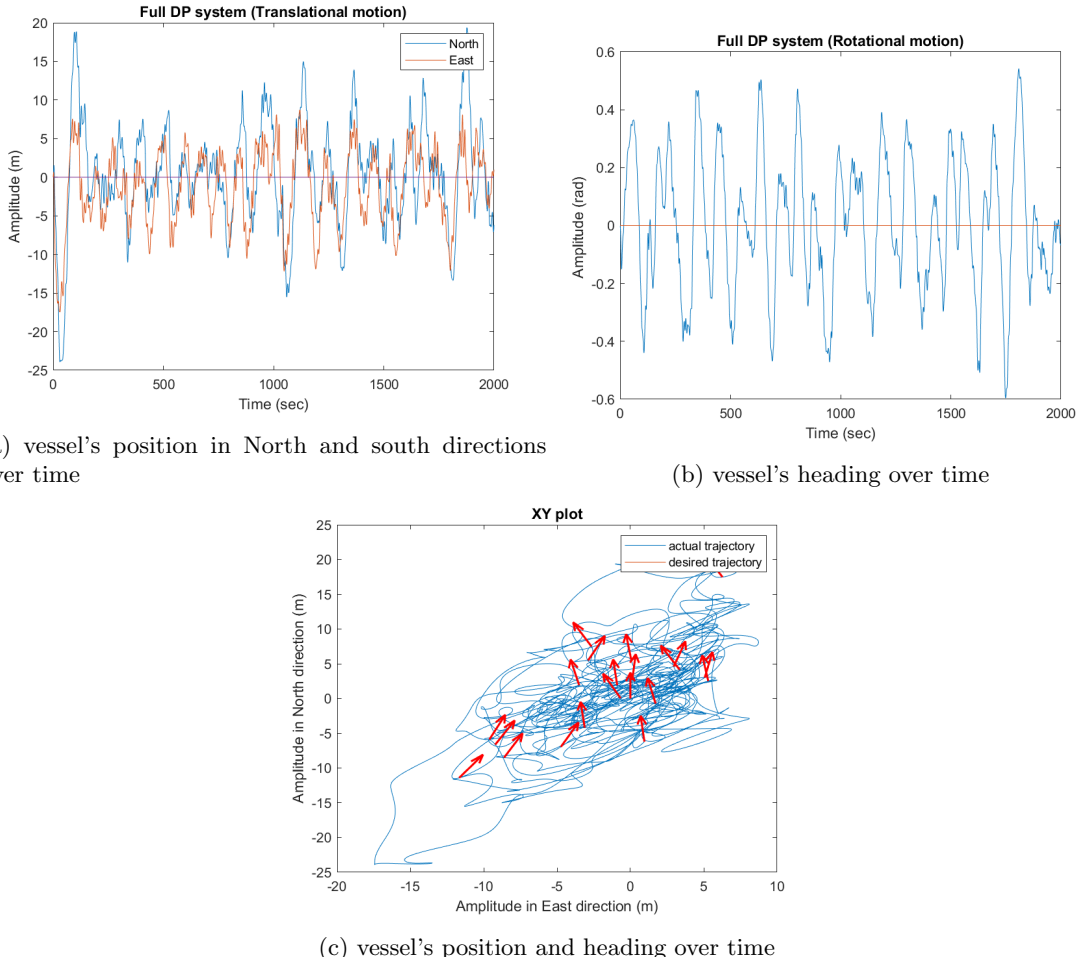


Figure 53: Full DP system performance in station keeping at $\eta = [000]$ test under full environmental loads, current, wind, and harsher waves, using NPO as an observer. The figures show the vessel's position η (North, East) as a blue curve and heading, represented by red arrows

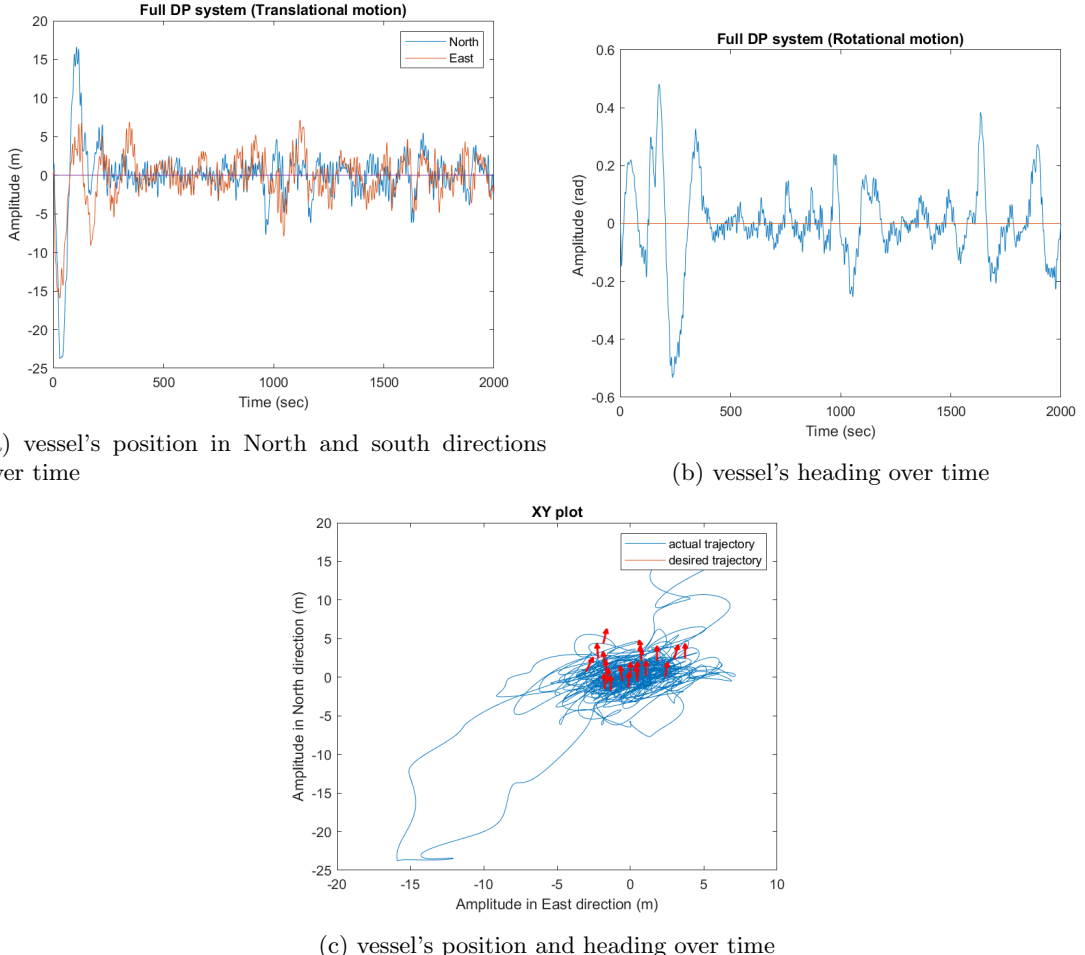


Figure 54: Full DP system performance in station keeping at $\eta = [000]$ test under full environmental loads, current, wind, and harsher waves, using EKF as an observer. The figures shows vessel's position η (North, East) as blue curve and heading , represented by red arrows

From the figures (52, 53, 54), it's apparent that the XY-plots in each simulation ((52c, 53c, 54c) is enough to assess the robustness.

- **No observer case in (52c):** has higher coverage of the space (very poor station keeping)
 - **Positions** mostly within a *30m in north & 20m in east*. This can be seen also in 52a
 - **Heading** has high variance as also apparent in 52b
- **NPO observer in (53c):** is same or slightly worse than the without observer case, according to this simulation.
 - **Positions** mostly within a *30m in north & 20m in east*. This can be seen also in 53a
 - **Heading** has higher variance as also apparent in 53b
- **EKF observer in (54c):** is the best performance.
 - **Positions** mostly within a *10m in north & 10m in east*. This can be seen also in 54a
 - **Heading** looking more up, but high variance as also apparent in 54b

From the previous comparison, even though the EKF can be further tuned, it shows superior performance than NPO and without observer case.

12 Conclusion

In this report, a full DP system is developed for a support vessel. After discussing the theoretical background and testing the recommended solution in simulation, based on Simulink and Marine control systems toolbox, various components of the system and their individual influence on the system is investigated.

The controller, specifically the PID controller, was selected for its robustness and simplicity in tuning. Tuning the PID controller was a recursive process, especially when integrating thruster dynamics into the system model, which required iterative adjustments to align control inputs with the operational capabilities of the thrusters. The performance of the selected controller and tuning parameters presented are satisfactory and investigate the capabilities and limitations of this thruster.

The reference model played a crucial role in the system's ability to chase after the desired set points, offering a smooth trajectory for the vessel to follow. Simulations showed that without the reference model, the system's response was less optimal, resulting in more substantial overshoots and longer settling times.

The observer, particularly the Extended Kalman Filter (EKF), was essential in providing accurate state estimations for the vessel, allowing the control system to compensate effectively for environmental disturbances. The EKF demonstrated superior performance over the Nonlinear Passive Observer (NPO) in both tracking accuracy and velocity estimation, especially in the presence of wave forces.

Thrust allocation was critical for ensuring that the control inputs were feasible within the physical constraints of the thrusters. It shows also the capability of the system to maintain good performance even if some thrusters are disabled, which is crucial for real-life scenarios. Our implementation of The pseudo-inverse method for thrust allocation proved to be more effective than our implemented thrust allocation method using quadratic programming method. Test carried out resulted in a smoother and more refined control with reduced fluctuations.

Environmental modeling was also a key aspect, as it allowed the system to predict and adapt to various disturbances. The simulations demonstrated the DP system's capability to maintain the vessel's pose under both fixed and changing current disturbances effectively.

Based on the simulations detailed in the report, the recommended settings for an optimal DP system would include the use of a PID controller for its robustness, an EKF for state estimation, and the pseudo-inverse method for thrust allocation. These components should be fine-tuned iteratively to align with the specific operational profile of the vessel and the environmental conditions it will encounter.

For future implementations, it is advised to ensure that the system can swiftly react to environmental forces to minimize deviations and maintain the vessel's set point. This may involve further tuning of the observer and the PID controller to enhance the system's response time and robustness.

References

- [1] Thor I. Fossen. *Handbook of Marine Craft Hydrodynamics and Motion Control*. John Wiley Sons, Ltd, 2011.